1969

Two and three pion production without annihilation in antiproton-proton interactions at 2.4 and 2.9 GeV/c

Richard Allen Jespersen
Iowa State University

TWO AND THREE PION PRODUCTION WITHOUT ANNIHILATION IN ANTIPROTON-PROTON INTERACTIONS AT 2.4 AND 2.9 GeV/c

by

Richard Allen Jespersen

A Dissertation Submitted to the

Graduate Faculty in Partial Fulfillment of

The Requirements for the Degree of

DOCTOR OF PHILOSOPHY

Major Subject: High Energy Physics

Approved:

Signature was redacted for privacy.

In Charge of Major Work

Signature was redacted for privacy.

Head of Major Department

Signature was redacted for privacy.

Dean of Graduate Faculty

Iowa State University
Of Science and Technology
Ames, Iowa

1969

TABLE OF CONTENTS

I. INTRODUCTION

Multiple pion production without annihilation in antiproton-proton interactions has been reported in bubble chamber experiments at antiproton laboratory momenta of 2.5 (1), 2.7 (2), 2.8 (3)[1], 3.28 (4-6), 3.6 (7-9), 3.66 (5, 6), 5.7 (9-12), and 7.0 (13) GeV/c. The cross-section for the double pion production reaction

$$\bar{p}p \rightarrow \bar{p}p\pi^+\pi^- \qquad (1)$$

is found to increase rapidly with beam momentum from 1.46 mb at 2.5 GeV/c to a maximum of 3.8 mb at 3.6 GeV/c, then decrease slowly.

A dominant feature of Reaction 1 at all of the above momenta is the presence of double resonance production. The reaction is found to proceed primarily through the intermediate quasi-two-body reaction

$$\bar{p}p \rightarrow \overline{\Delta^{++}}\,\Delta^{++}, \quad \Delta^{++} \rightarrow p\pi^+, \quad \overline{\Delta^{++}} \rightarrow \bar{p}\pi^- \qquad (2)$$

Here Δ^{++} is the P_{33} [P-wave, I = 3/2, $J^P = (3/2)^+$] baryon resonance having a central mass of 1236 MeV and a width of 120 MeV, and decaying 100% to $p\pi^+$. The importance of this double resonance production is seen in the dominance of Reaction 1 by nearly 100% $\overline{\Delta^{++}}\,\Delta^{++}$ production near the $\overline{\Delta^{++}}\,\Delta^{++}$ threshold of 2.0 GeV/c. In fact, Reaction 1 has not been observed below 2.0 GeV/c, even though its threshold is 1.2 GeV/c (14).

A second prominent feature of the reaction is a sharp peaking at small angles in the distribution of the production angle, defined as the angle

---

[1] The reaction reported here was $\bar{p}p(n) \rightarrow \bar{p}p\pi^+\pi^-(n)$, using a deuterium target.

between the incoming $\bar{p}$ and the outgoing $\bar{p}\pi^-$ system in the over-all center-of-mass. This peripheral character of the reaction suggests the possibility of interpreting the interaction in terms of a long range force or, equivalently, the exchange of a light particle, the pi meson. The one-meson-exchange model has become widely used for the calculation of cross-sections, invariant mass distributions, angular distributions, and decay angular correlations for peripheral meson-nucleon and nucleon-nucleon interactions. Explicit calculations can be done easily for quasi-two-body reactions (15-17), so Reaction 2 offers an appropriate test of the model.

At the time this study was begun, the only near-threshold investigations of Reaction 1 reported were the previous Iowa State University experiment of Crawley et al. (2) at 2.7 GeV/c and the experiment of Ferbel et al. (4-5) at 3.28 GeV/c. At the lower momentum, Reaction 1 had been found to proceed 100% through the intermediate reaction (Reaction 2), while this double resonance production had been found to account for 80% of the Reaction 1 events at the higher momentum. The one-pion-exchange model had been found to give reasonably good predictions of the $p\pi^+$ and $\bar{p}\pi^-$ invariant mass distributions and of the distribution of Δ^2, the four-momentum transfer from the incoming $\bar{p}$ to the outgoing $\bar{p}\pi^-$ system. However, at 2.7 GeV/c, the model did not predict the decay angular distributions correctly, and the $\rho_{1,1}$ spin-density matrix element (not calculated at 3.28 GeV/c) was found to have a strong Δ^2 dependence not predicted by the model.

It was decided to investigate the near-threshold energy dependence of these effects by taking data at momenta on both sides of 2.7 GeV/c. The

momenta chosen were 2.4 and 2.9 GeV/c, with 50% more pictures to be taken at the lower momentum because of the anticipated rapid decrease of the Reaction 1 cross-section with decreasing beam momentum. These data would provide tests of the one-pion exchange model and perhaps suggest additional model calculations.

Presented here is an investigation of Reaction 1 at 2.4 and 2.9 GeV/c and comparisons of the intermediate reaction (Reaction 2) with the one-pion-exchange model predictions. The near-threshold energy dependence is examined, including the data from the previous experiment at 2.7 GeV/c. Also presented are the cross-sections for the triple pion production reactions

$$\bar{p}p \rightarrow \bar{p}pp\pi^+\pi^-\pi^o \tag{3}$$

$$\bar{p}p \rightarrow \bar{p}pn\pi^+\pi^+\pi^- \tag{4}$$

$$\bar{p}p \rightarrow \bar{n}pp\pi^-\pi^-\pi^+. \tag{5}$$

Preliminary reports of this investigation at 2.9 GeV/c (18-20) and of other final states in these experiments (21) have been presented elsewhere.

The experimental procedure is discussed in Section II. The experimental results are given in Sections III and IV, and these are compared with the predictions of the one-pion-exchange model in Section V. Section VI is a summary of the present and previous experiments on Reaction 1.

II. EXPERIMENTAL PROCEDURE

The following discussion is a description of the details of the experiment, from the accelerator run to the selection of final data samples. The experimental run and the beam properties are described briefly in Part A, while the scanning and measuring are discussed in Part B. Part C is devoted to an explanation of the procedures used for kinematic fitting and the selection of events, and Part D lists the tests which were made to insure that the final data samples were free of biases.

A. The Accelerator Run and Beam Properties

The Brookhaven National Laboratory 31-in. hydrogen bubble chamber was exposed to an electrostatically separated beam of 2.9 GeV/c antiprotons and, subsequently, to one of 2.4 GeV/c. In tuning the beam, a clear separation of the pions, kaons, and antiprotons was seen at both momenta, insuring that a reasonably pure sample of antiprotons reached the bubble chamber. In addition, the purity of the beam was monitored by a Čerenkov counter which recorded pions and muons. At each momentum, this procedure resulted in a beam which was estimated to be more than 99% antiprotons, and no corrections were made for beam contamination.

The beam flux entering the bubble chamber was monitored by a scintillation counter. In order to obtain pictures having maximum numbers of beam tracks consistent with ease of scanning and measuring, this counter was required to indicate a pulse of between six and sixteen particles before a picture was taken. This flux was determined more precisely at scanning time by counting the number of beam tracks in every tenth frame of the film. (Only those tracks entering the fiducial volume used were included in this

count.) The flux was found to be 8.8 beam tracks per picture at each momentum.

At the beginning of the data analysis, the momentum of the beam used in the fitting procedure was the value determined from the field settings in the magnets used to direct the beam into the chamber. In order to get more precise values, the events accepted as due to Reaction 1 at each momentum were reprocessed, treating the momentum of the beam as unknown. These events were used because the masses of all the particles in the reaction were known. The calculations were otherwise independent of the previous fitted values. The distributions of the fitted beam momenta resulted in values of 2375 ± 75 and 2885 ± 80 MeV/c for the two data samples. All measured events were then reprocessed using these values.

B. Scanning and Measuring

Totals of 58,277 pictures at the lower momentum and 37,189 at the higher were scanned for four-prong events, resulting in samples of 17,613 and 10,246 events, respectively, in the fiducial volume used. Approximately 10,000 pictures at each momentum were scanned a second time to determine the efficiency of locating four-prong events. It was determined that the first scan was 88% efficient at 2.4 GeV/c and 92% at 2.9 GeV/c. Only those events found in the first scan were included in the samples of events measured. As is shown in Part D, this did not result in biased data samples.

The four-prong events measured totaled 15,965 at 2.4 GeV/c and 9393 at 2.9 GeV/c. These events were measured in three stereoscopic views, with the results recorded on punched cards. The remaining four-prong events

found in the scan were determined to be unmeasurable in one or more views due to very faint tracks, flash spots on the film, very large numbers of tracks in the picture, or other reasons.

It was necessary to remeasure some of these events after the reconstruction and fitting had been done. The reasons for this are discussed in Part C. A few of these events to be remeasured at 2.9 GeV/c, and all of them at 2.4 GeV/c, were reprocessed on the new on-line measuring system (22). Instead of the output of the measuring machines being punched on cards, it was sent directly to a computer. The reconstruction in space and a few of the fitting attempts were done immediately, and the measurer was instructed by the computer either to measure the event again or to go on to the next event. These instructions were based on the size of errors in the reconstruction and on comparisons of proton and antiproton identifications (see Part C) made by the measurer to the particle types in the fits obtained. If there were large errors or if an event had an identified particle but no corresponding fit, the computer asked that the event be remeasured.

C. Fitting and Event Selection

1. Criteria of fits

Each measured event was reconstructed in space and kinematically fitted using the program GUTS (23, 24). An attempt was made to fit each event to all mass hypotheses for four or five particles in the final state consistent with the selection rules of the strong interactions. In this fitting procedure, the quantity chi-squared, which is a measure of the confidence level of a fit, is defined by (24)

$$\chi^2 = \sum_{i=1}^{5} \sum_{j=i}^{3} \left[\frac{A_{ij} - B_{ij}}{\Delta A_{ij}} \right]^2 , \text{ where}$$

A_{i1} is the measured azimuthal angle, A_{i2} is the tangent of the measured dip angle, and A_{i3} is the measured curvature, defined as [momentum X cos (dip)]$^{-1}$, for the i^{th} track (beam and four outgoing tracks). The quantities ΔA_{ij} are the corresponding uncertainties in the measured quantities, and B_{ij} are the corresponding fitted values. The missing mass for a given reaction hypothesis is defined as

$$(MM)^2 = [E_o - (\sum_{i=1}^{4} E_i)]^2 - [\vec{P}_o - (\sum_{i=1}^{4} \vec{P}_i)]^2,$$

where E_o and $\vec{P}_o$ are the total energy and momentum of the initial $\bar{p}p$ system, and E_i and $\vec{P}_i$ are the total energy and momentum of the i^{th} outgoing track. For a particular mass assignment M_i, E_i is determined from the measured momentum using $E_i^2 = P_i^2 + M_i^2$.

An event was said to have a fit to Reaction 1 if the missing mass differed from zero by less than four standard deviations and if chi-squared was less than 31. An event was said to have a fit to any of the Reactions 3 through 5 if the missing mass differed from the mass of the postulated neutral particle by less than four standard deviations and if chi-squared was less than 13. It was found that using more restrictive criteria eliminated real fits, while less restrictive ones merely included more simulated fits in the data samples.

2. Elimination of ambiguities

Each event which had a fit to any of Reactions 1, 3, 4, or 5 was checked for ionization consistence of all the outgoing tracks. Since the

bubble density of a track is inversely proportional to the square of the particle velocity, particles of the same momentum but different mass leave tracks of different bubble density. A fit was said to be ionization consistent if the mass assignment of no track could be ruled out on the basis of bubble density as determined by comparing the brightness of each track to that of the beam track, which is nearly minimum ionizing. This proved to be a strong requirement for Reactions 1 and 3. It was possible to positively identify either the proton or the antiproton in more than 90% of the events having fits to Reaction 1 at both 2.4 and 2.9 GeV/c. For events which had multiple fits to Reactions 1 and/or 3, this identification was usually sufficient to eliminate the ambiguities.

Although nearly every event which had a fit to Reaction 1 was accepted as being due to that reaction, there were many simulated fits to Reactions 3, 4, and 5, where one particle was unmeasured. In particular, events due to Reaction 1 frequently had simulated fits to Reaction 3 in which the center-of-mass momentum of the fitted π^o was close to zero. So an additional requirement for acceptance of fits to Reaction 3 was that the center-of-mass momentum of the π^o be greater than 100 MeV/c. It was also required that the missing mass be within 0.024 $(GeV)^2$ of the square of the π^o mass, and that chi-squared be less than 2.0. These cuts were determined from examination of a scatter plot of the chi-squared versus missing mass squared distributions for all fits to Reaction 3. These requirements eliminated all ambiguities which had remained among the ionization consistent fits to Reactions 1 and 3.

Many of the Reaction 4 and 5 events, for which only one of the two

nucleons is observable, had no positively identifiable antiproton or proton. This was particularly true of Reaction 4 events, since the antiproton tends to have a high momentum. For these reactions there was a much greater degree of ambiguity than for the others. In order to determine which fits were real, an attempt was made to estimate the chi-squared and missing mass squared distributions to be expected from fits to reactions with an unseen nucleon. This study consisted of reprocessing all the 2.9 GeV/c events which had been accepted as due to Reaction 1. Fits were attempted to the reactions

$$\bar{p}p \rightarrow \bar{p}(p)\pi^+\pi^- \tag{6}$$

$$\bar{p}p \rightarrow (\bar{p})p\pi^+\pi^-, \tag{7}$$

where the particles in parentheses were treated as unmeasured. These were taken to be good approximations to reactions 4 and 5, respectively, in the sense of having a particle of similar mass and momentum unmeasured. It was found by examining scatter plots of chi-squared versus missing mass squared that 88% of the Reaction 6 events had missing mass squared differing from the square of the proton mass by less than 0.16 $(\text{GeV})^2$ and had chi-squared less than 2.0. The corresponding values for Reaction 7 were 0.12 $(\text{GeV})^2$ and 4.0, the differences being due to the tendency of the former reaction to have a high momentum antiproton, while the latter more often has a low momentum proton. The curvature of the lower momentum track can be measured more accurately, resulting in a smaller uncertainty in the denominator of chi-squared. These values were then used (along with ionization consistence) as the criteria for acceptance of fits to Reactions 4 and 5, respectively, at both 2.4 and 2.9 GeV/c. It was estimated that the

events with accepted fits to Reactions 3, 4, or 5 constituted approximately 90% of all the measured events due to those reactions.

3. Remeasuring

It was necessary to measure some events a second time in order to obtain acceptable fits. An event was remeasured if the reconstruction failed or had very large errors, if the fitting to Reactions 1, 3, 4, or 5 resulted in the reduction of constraints, or if there was an identified antiproton or proton but no corresponding acceptable fit.

4. Selection of final data samples

Fits which passed all of the above requirements were subjected to one final test. In order to eliminate fits which were not associated with true beam tracks or which resulted from poorly measured events, restrictions were made on the momentum and angles of the incident beam particle. These restrictions were determined from examination of the corresponding distributions for all four-prong events. The momentum was required to be within 165 MeV/c of the appropriate value reported in Part A for each data sample. The dip was required to be within 5 degrees of zero, and the azimuth as a function of the vertex position along the incident beam direction was required to be within the box shown in Figure 1a at 2.4 GeV/c and Figure 1b at 2.9 GeV/c (for simplicity in plotting, only 5,000 events were included in each sample). These cuts eliminated 1.6% of the accepted fits to Reaction 1 at each momentum.

In Table 1 are shown the numbers of events accepted as due to Reactions 1, 3, 4, and 5 at each momentum, the remaining events being due to the many other possible final states having four charged particles (some of these are

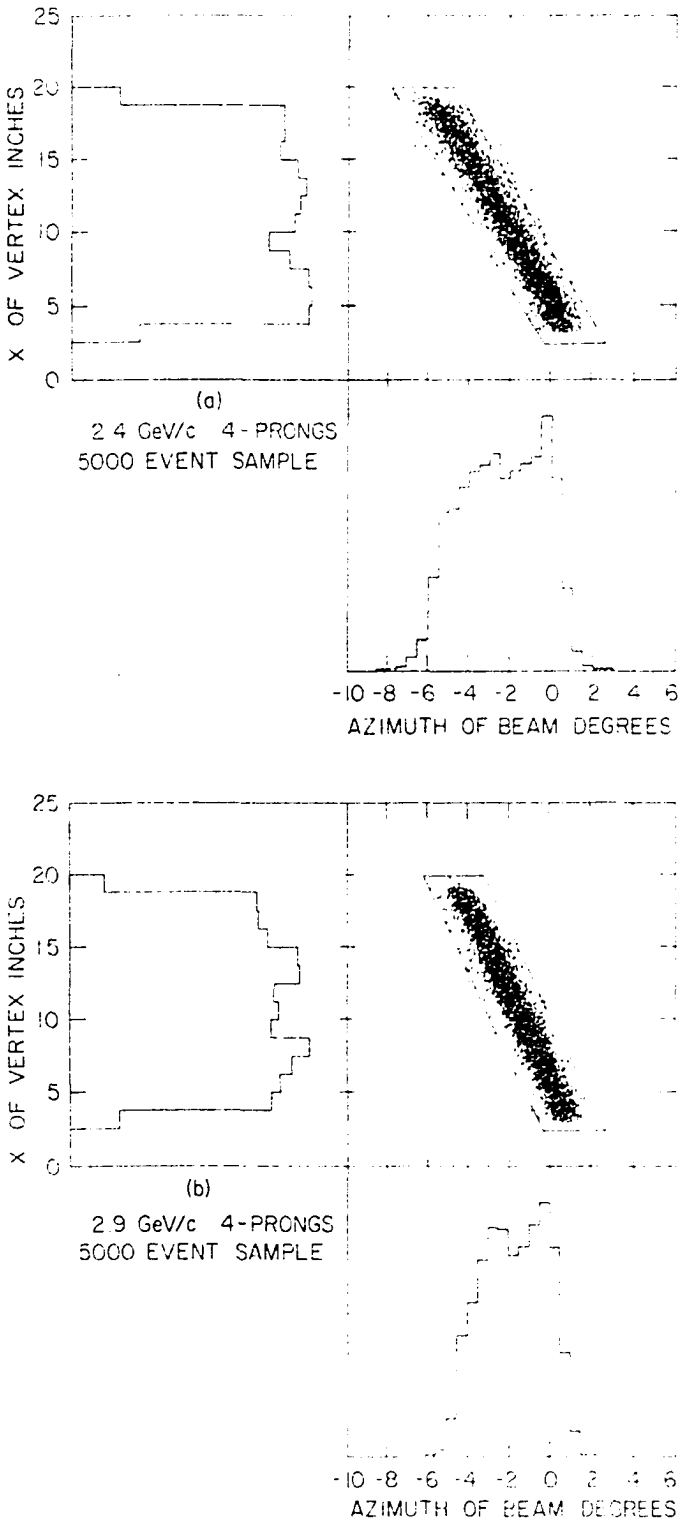

Figure 1 Scatter plots of the beam azimuth versus the position of the vertex along the incident beam direction. The boxes indicate the restrictions used in determining the final data samples.

discussed in Reference 21). The chi-squared distributions for the events accepted as due to Reaction 1 at 2.4 and 2.9 GeV/c are shown in Figures 2a and 2b, respectively.

Table 1. Numbers of events accepted

	2.4 GeV/c	2.9 GeV/c
$\bar{p}p\pi^+\pi^-$	897	1015
$\bar{p}p\pi^+\pi^-\pi^o$	6	46
$\bar{p}n\pi^+\pi^+\pi^-$	8	53
$\bar{n}p\pi^-\pi^-\pi^+$	10	47

D. Tests for Biases

Approximately 40 to 45 events at each momentum had an identified $\bar{p}$ or p but no acceptable fit to any of Reactions 1, 3, 4, or 5. These events were considered to be due to Reaction 1 for the purpose of cross-section calculations, since statistics favor this over the other reactions in which there is a $\bar{p}$ or p in the final state. These events, along with the Reaction 1 events not found in the scanning, account for a significant fraction of all the Reaction 1 events, and indicate the possibility of biases in the final data samples. This possibility was examined by looking for apparent violations of C or CP invariance in all of the distributions examined which are subject to such tests (25). Here C is the charge conjugation operator, and P is the parity operator. The following distributions were compared for consistency with C invariance:

1) The center-of-mass momentum distributions of the π^- and π^+ are

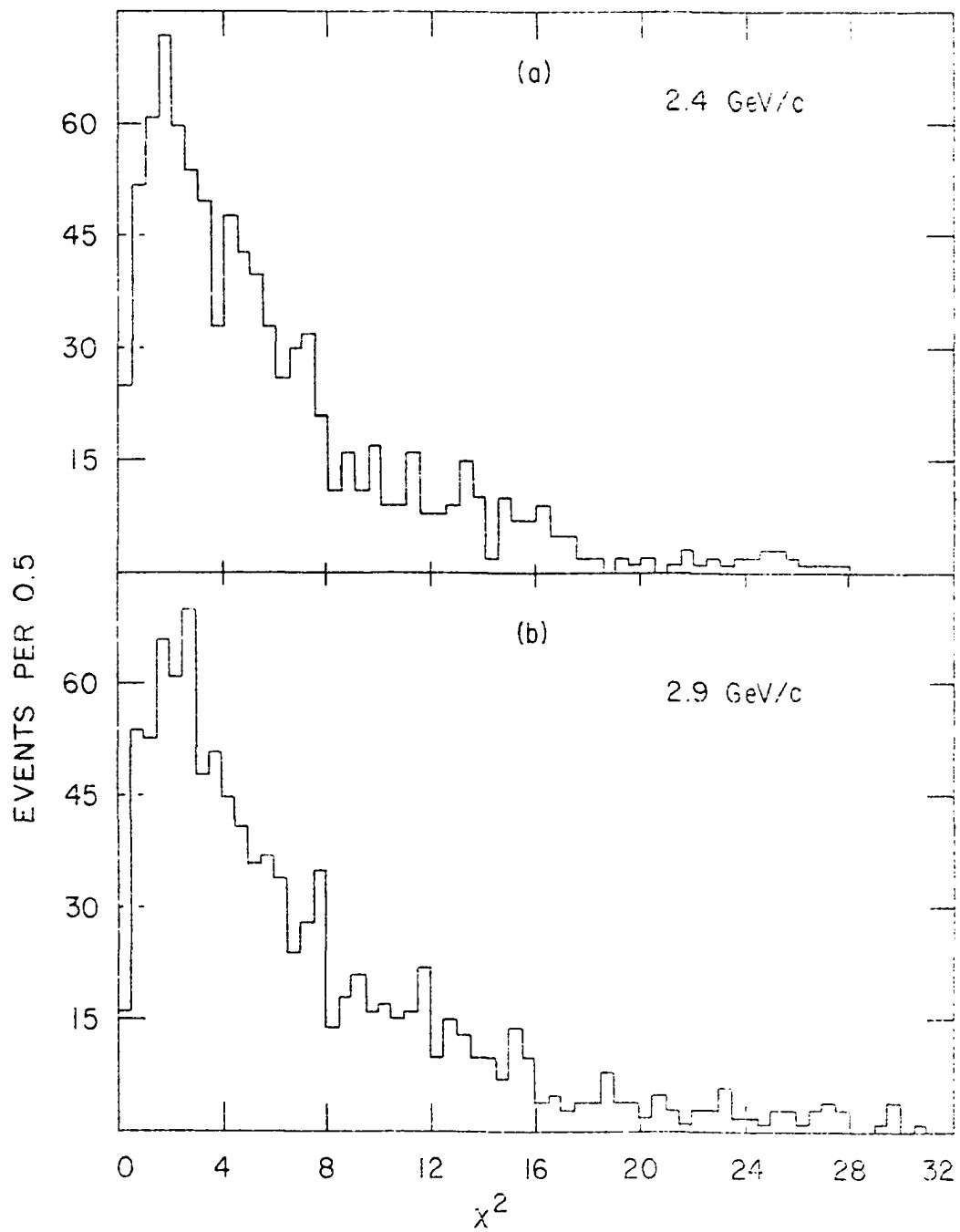

Figure 2. Chi-squared distributions for the fits accepted as due to Reaction 1.

shown in Figure 3. They should be the same.

2) The center-of-mass momentum distributions of the outgoing $\bar{p}$ and p are shown in Figure 4. They should be the same.

3) The center-of-mass angular distributions of the π^- and π^+ with respect to the incident $\bar{p}$ are shown in Figure 5. They should be the same if one is reflected about $\cos\theta = 0$.

4) The center-of-mass angular distribution of the outgoing $\bar{p}$ and p are shown in Figure 6. The test is the same as in 3).

5) The invariant mass distributions which should be the same are $\bar{p}p\pi^-$ and $p\bar{p}\pi^+$, $\bar{p}\pi^-\pi^+$ and $p\pi^+\pi^-$, $\bar{p}\pi^-$ and $p\pi^+$, and $\bar{p}\pi^+$ and $p\pi^-$. These distributions were also examined. They are presented in Sections IV and V.

An additional test of C and CP invariance is shown in Figures 7 and 8. The angle $\phi(\bar{p},\pi^-)$ between the projections of the final $\bar{p}$ and π^- momenta onto the plane perpendicular to the incoming $\bar{p}$ momentum in the center-of-mass system is shown in Figure 7. The distributions of $\phi(\bar{p},\pi^-)$ are shown in Figures 8a and 8c, while the corresponding distributions for the final p and π^+ are shown in Figures 8b and 8d. CP invariance requires the $\bar{p}\pi^-$ and $p\pi^+$ distributions to be identical, and the addition of C invariance requires each to be symmetric about 180°. All of the above requirements are satisfied within statistical limits at both beam momenta, indicating that the final data samples for Reaction 1 are unbiased in this respect.

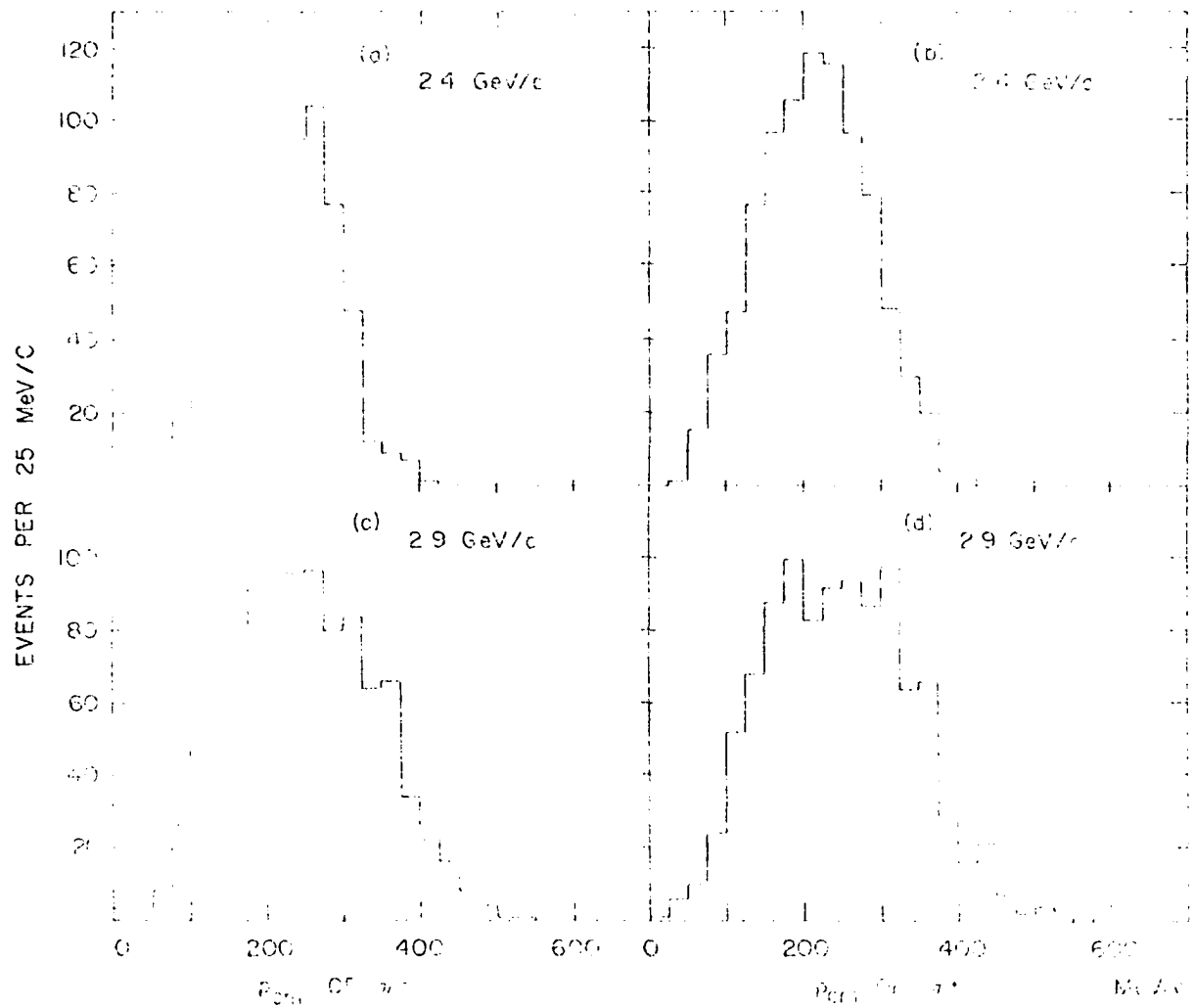

Figure 3. The center-of-mass momentum distributions of the outgoing π^- and π^+ for Reaction 1.

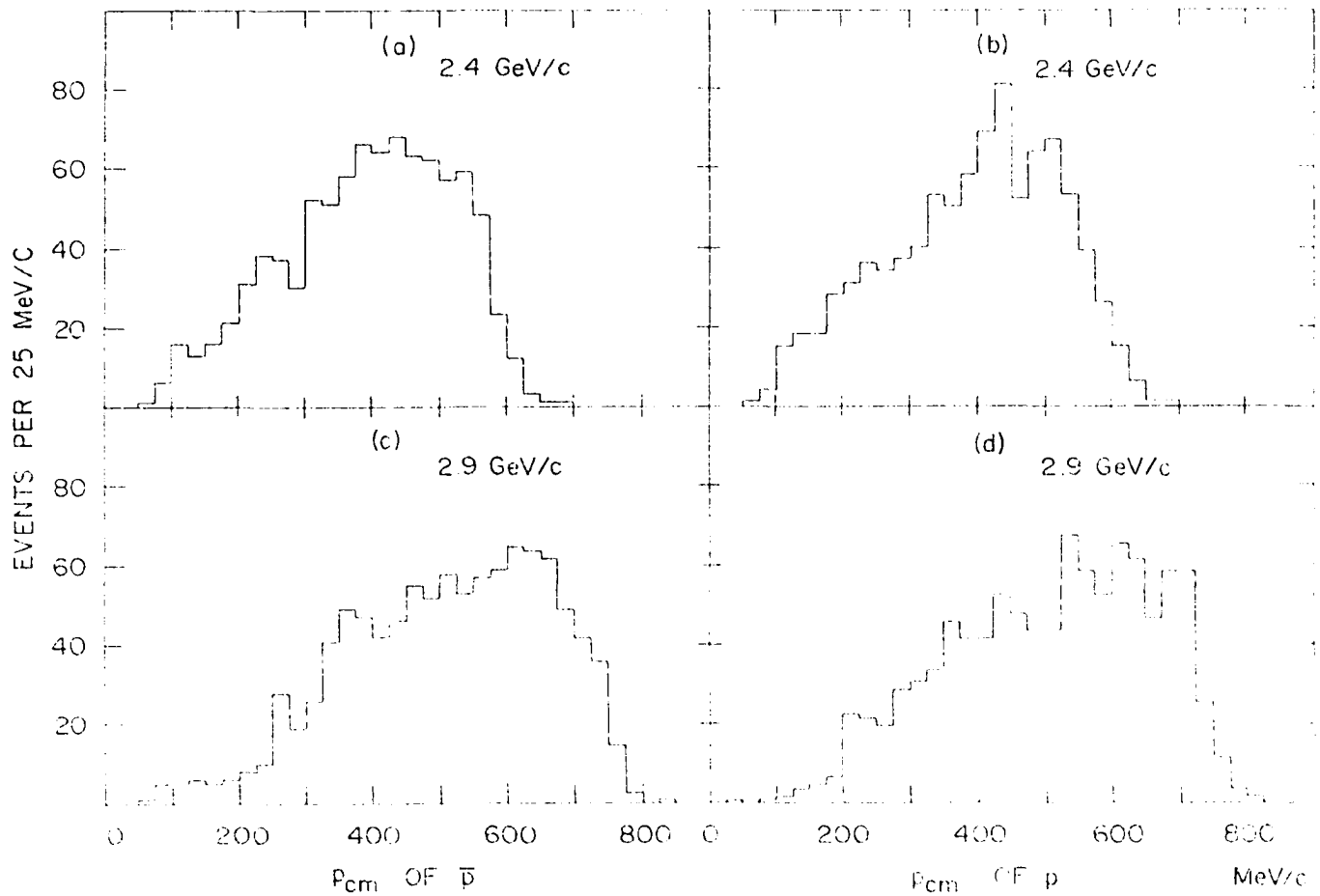

Figure 4. The center-of-mass momentum distributions of the outgoing $\bar{p}$ and p for Reaction 1

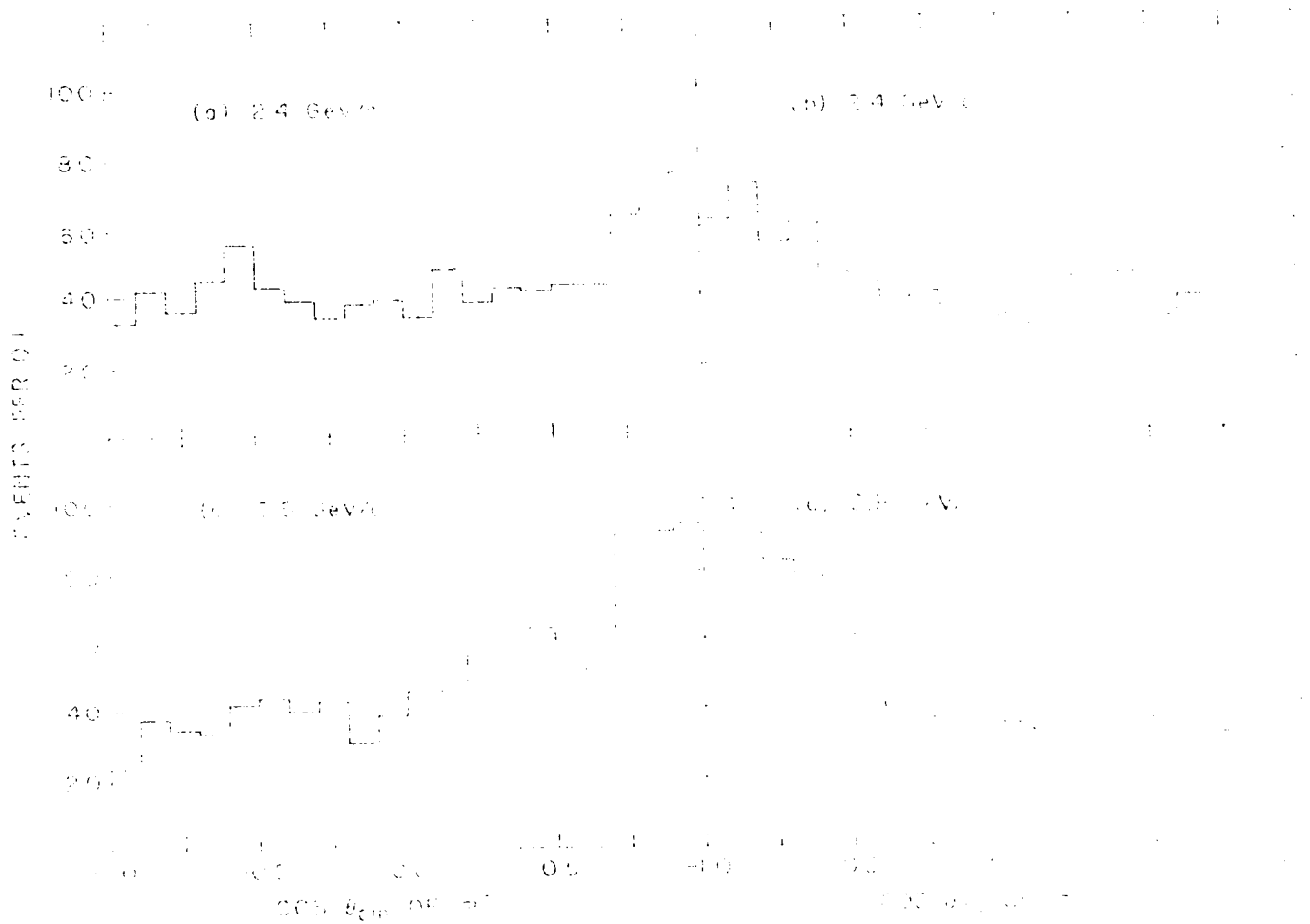

Figure [illegible] Two proton-deuteron angular distributions of the outgoing [illegible] respect to the incident [illegible]

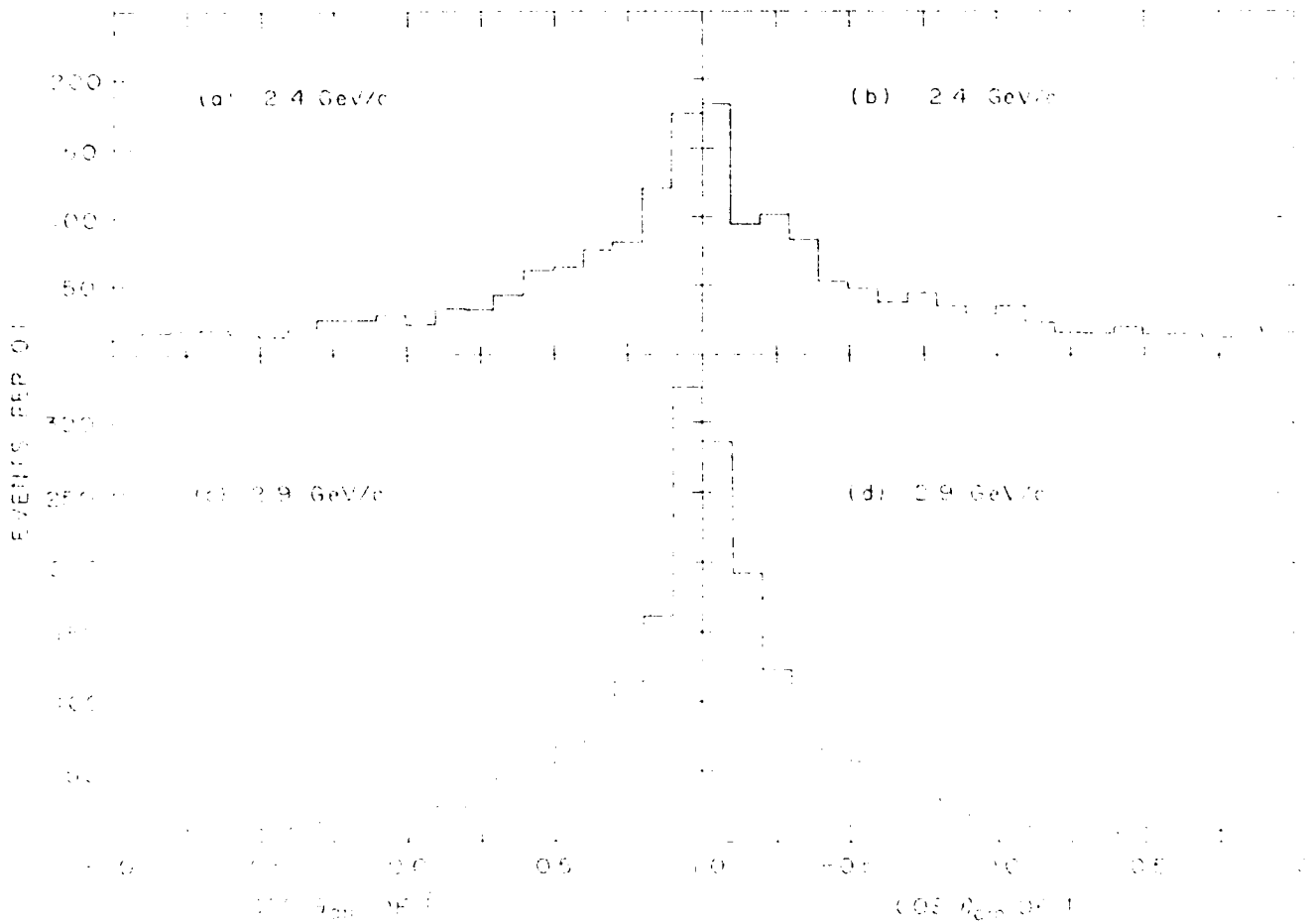

Figure ... The ... angular distribut... the outgoing $\bar{\Sigma}$ and ... of ... with respect to the incident $\bar{p}$

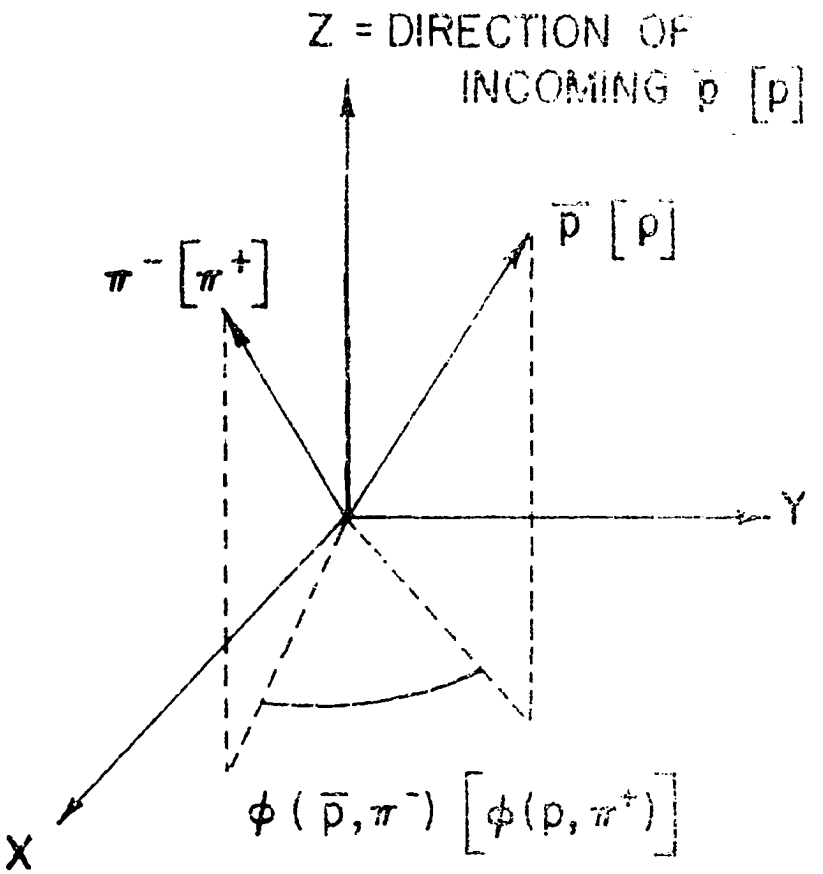

Figure 7. Definition of the center-of-mass angle $\phi(\bar{p},\pi^-)$ for Reaction 1.

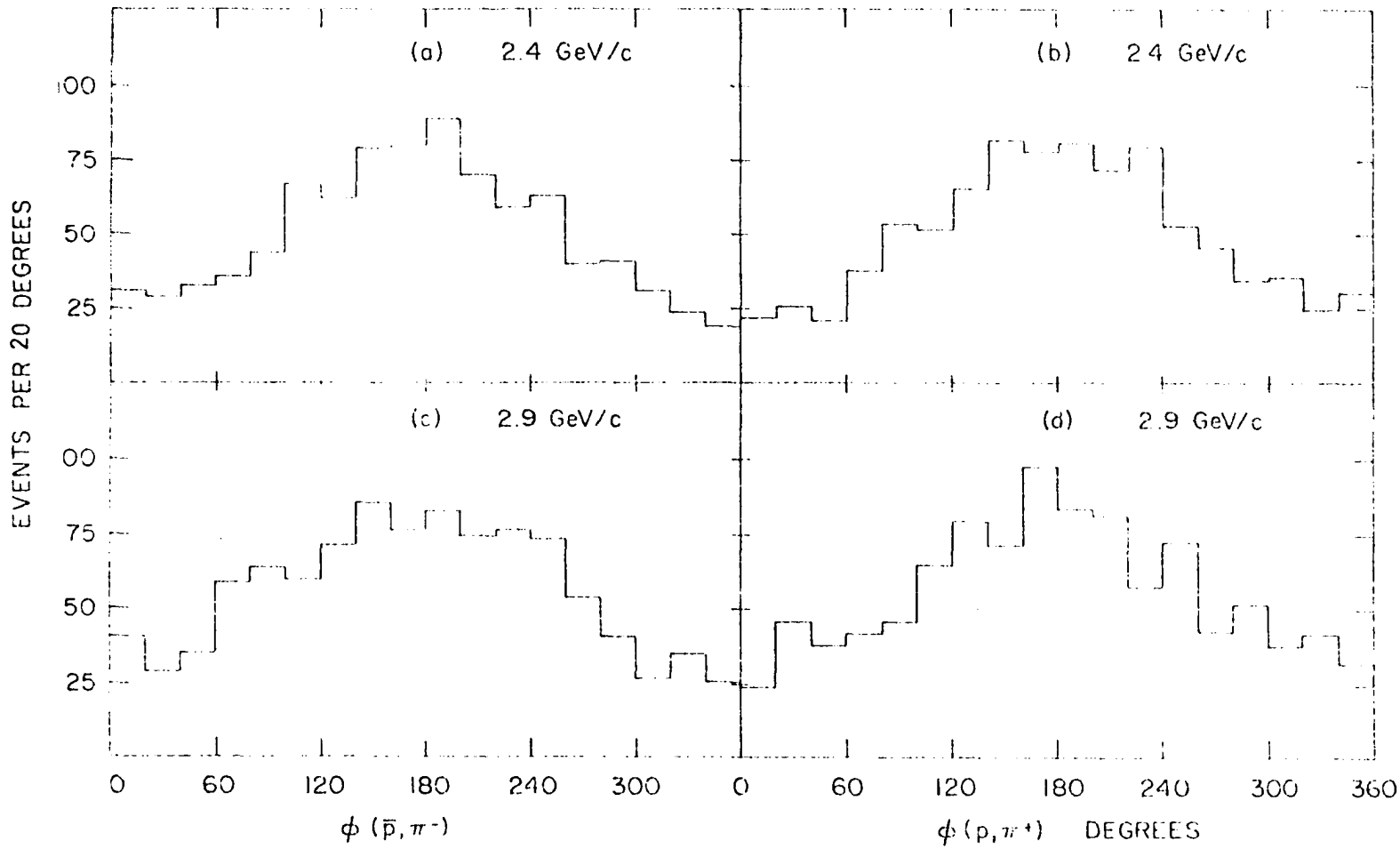

Figure 8. The $\phi(\bar{p},\pi^-)$ and $\phi(p,\pi^+)$ distributions for Reaction 1.

III. CROSS-SECTIONS

The cross-sections for a particular reaction can be determined from

$$N = N_o \sigma (N_c \ell),$$

where N is the number of reactions, N_o is the number of incoming beam particles, σ is the cross-section, and $N_c \ell$ is the number of target centers per unit area. This can be conveniently expressed as

$$[N_m/SR] = [N_t N_p] \sigma [\rho (N_a/A) \ell],$$

where N_m is the number of measured events for this reaction, S is the scanning efficiency, and R is the ratio of the number of four-prong events measured to the number found in the scan. N_t is the number of beam tracks per picture and N_p is the number of pictures scanned, while ρ is the density of hydrogen in the bubble chamber, N_a is Avagadro's number, A is the atomic weight of hydrogen, and ℓ is the average length of the interacting beam tracks in the fiducial volume used.

The length ℓ was found from the distributions of the vertex position in the bubble chamber, while ρ was determined from measurements of the length of muons in $\pi\mu e$ decays and the known range of muons in hydrogen as a function of density. These and the remaining quantities (from Section II) needed to calculate the cross-sections are summarized in Table 2, where the numbers of events N_m are corrected for the losses discussed in Section II. The resulting cross-sections for Reactions 1, 3, 4, and 5 are given in Table 3.

Table 2. Data for cross-section calculations

	2.4 GeV/c	2.9 GeV/c
$N_m(\bar{p}p\pi^+\pi^-)$	940	1058
$N_m(\bar{p}p\pi^+\pi^-\pi^o)$	7	51
$N_m(\bar{p}n\pi^+\pi^+\pi^-)$	9	59
$N_m(\bar{n}p\pi^-\pi^-\pi^+)$	11	52
N_t	8.8	8.8
N_p	58,277	37,189
S	0.88	0.92
R	15,965/17,613	9,393/10,246
ρ	0.0658 ± 0.0005 gm/cm^3	
N_a	6.025×10^{23} atoms/atomic weight	
A	1.008 gm/atomic weight	
ℓ	15.61 ± 0.37 in.	15.24 ± 0.25 in.

Table 3. Cross-sections

	2.4 GeV/c	2.9 GeV/c
$\bar{p}p\pi^+\pi^-$	1.48 ± 0.07 mb	2.53 ± 0.10 mb
$\bar{p}p\pi^+\pi^-\pi^o$	10 ± 5 μb	122 ± 40 μb
$\bar{p}n\pi^+\pi^+\pi^-$	14 ± 10	141 ± 70
$\bar{n}p\pi^-\pi^-\pi^+$	17 ± 10	125 ± 70

IV. THE $\bar{p}p\pi^+\pi^-$ FINAL STATE

The numbers of events due to Reactions 3, 4, and 5 are so small that no further study of these reactions was attempted. The remainder of this report is devoted to the investigation of Reaction 1. The invariant mass distributions are presented in Part A, along with an analysis to determine the amounts of $\bar{\Delta}^{--}$ and Δ^{++} resonance production. The angular distributions of production of these resonances are given in Part B, and their decay angular distributions are shown in Part C. The spin-density matrix elements, which are related to the decay angular distributions, are also presented in Part C. The joint density matrix elements from the 2.7 GeV/c data (which were not previously calculated) are included.

A. *Invariant Mass Distributions and Resonance Production*

The square of the invariant mass of a combination of n particles is defined by

$$M^2_{1\ldots n} = \left(\sum_{i=1}^{n} E_i\right)^2 - \left(\sum_{i=1}^{n} \vec{P}_i\right)^2,$$

where E_i ($E_i^2 = \vec{P}_i^{\,2} + M_i^2$) is the energy and $\vec{P}_i$ is the momentum of the i^{th} particle. If these n particles are the decay products of a resonance produced in some fraction of the events, the invariant mass distribution will have a peak near the mass of the resonance.[1] If the resonance is produced in only a small fraction of the events, this peak may be only a small bump on an otherwise smooth distribution, or it may be difficult to distinguish from the statistical fluctuations. On the other hand, if resonance produc-

---

[1] If a resonance is broad, the energy dependence of the width can cause the observed peak to fall below the resonance mass. Jackson (26) discusses this effect in detail.

tion accounts for a large part of the events, the invariant mass distribution may be dominated by the resonance peak. Examples of the latter are shown in Figure 9, two-dimensional scatter plots of the invariant masses of the outgoing $\bar{p}\pi^-$ and $p\pi^+$ combinations. Each of these mass distributions is strongly peaked at about 1220 MeV. The clustering of each scatter plot about the overlap region shows the dominance of simultaneous resonance production at both 2.4 and 2.9 GeV/c, i.e., Reaction 1 proceeds primarily through the intermediate Reaction 2.

In order to determine just what fraction of the reaction goes through this intermediate state at each momentum, fits were done to the scatter plots of Figure 9. Since the resonances can be produced doubly, singly, or not at all, the theoretical expression for these invariant mass distributions was written as a sum of expressions for each of these possibilities. The form used is

$$L(\bar{\omega},\omega) = \alpha(\bar{p}\pi^- p\pi^+)\ F(\bar{p}\pi^- p\pi^+) + \alpha(\bar{\Delta}p\pi^+)\ F(\bar{\Delta}p\pi^+) + \alpha(\bar{p}\pi^-\Delta)\ F(\bar{p}\pi^-\Delta) + \alpha(\bar{\Delta}\Delta)\ F(\bar{\Delta}\Delta). \quad (8)$$

In this expression $\bar{\omega}(\omega)$ is the invariant mass of the outgoing $\bar{p}\pi^-$ ($p\pi^+$) combination, the α's are the fractions of the events of the types indicated by the arguments (e.g., $\alpha(\bar{\Delta}\Delta)$ is the fraction of Reaction 1 going through the intermediate Reaction 2), and the F's are phenomonological expressions representing the production and decay of the state indicated by the arguments (e.g., $F(\bar{\Delta}\Delta)$ represents phase space production of a $\bar{\Delta}^{++}$ Δ^{++} state followed by Breit-Wigner decay of that state to $\bar{p}\pi^-$ $p\pi^+$). These F's are given by (2, 26)

$$F(\bar{p}\pi^- p\pi^+) = C_1 \frac{P(\bar{\omega};M^2,m^2)}{\bar{\omega}} \frac{P(\omega;M^2,m^2)}{\omega} \frac{P(E;\bar{\omega}^2,\omega^2)}{E} \bar{\omega}\omega$$

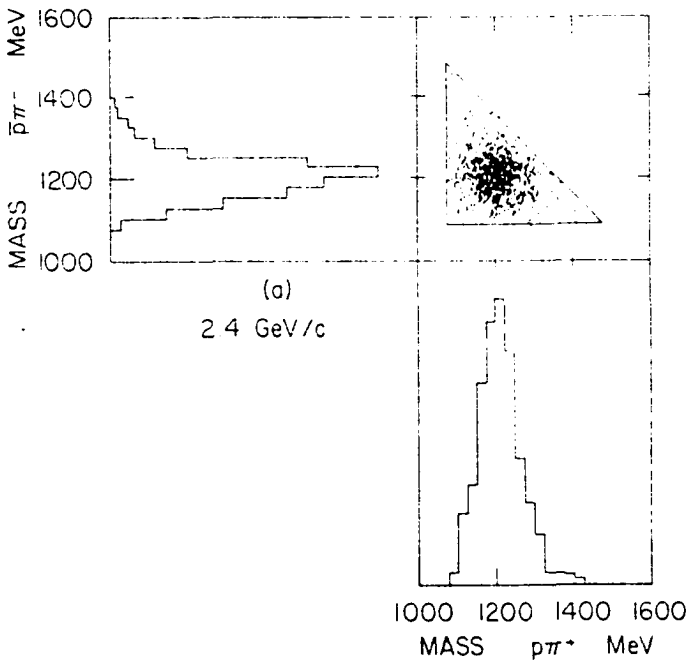

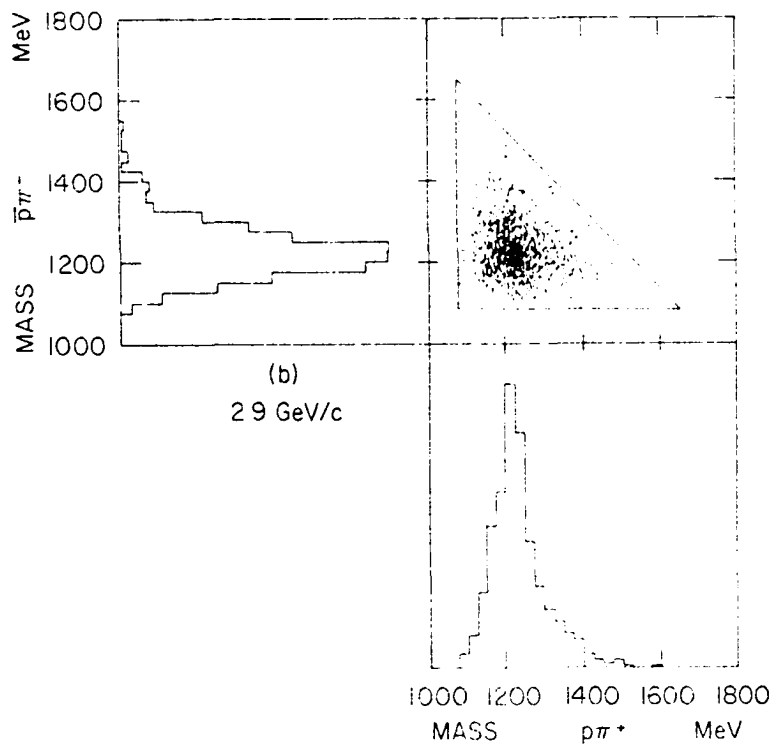

Figure 9. Scatter plots of the $p\pi^+$ versus the $\bar{p}\pi^-$ invariant mass distributions. The kinematic limits are indicated by the solid lines.

$$F(\bar{\Delta}p\pi^+) = C_2\, F(\bar{p}\pi^- p\pi^+)\; \varphi\,(\bar{\omega})$$

$$F(\bar{p}\pi^- \Delta) = C_3\, F(\bar{p}\pi^- p\pi^+)\; \phi\,(\omega)$$

$$F(\bar{\Delta}\Delta) = C_4\, F(\bar{p}\pi^- p\pi^+)\; \varphi\,(\bar{\omega})\; \varphi\,(\omega),$$

where the C's are normalization constants, M(m) is the nucleon (pion) mass, and E is the total energy in the over-all center-of-mass system. $P(\omega;M^2,m^2)$ is the magnitude of the final π^+ momentum in the final $p\pi^+$ rest frame, given as

$$P(\omega;M^2,m^2) = (2\omega)^{-1}\left[\omega^4 - 2\omega^2(M^2 + m^2) + (M^2 - m^2)^2\right]^{\frac{1}{2}}.$$

Here $F(\bar{p}\pi^- p\pi^+)$ is the four-body phase-space distribution representing the probability of production of the $\bar{p}\pi^- p\pi^+$ final state such that the $\bar{p}\pi^-(p\pi^+)$ combination has invariant mass $\bar{\omega}(\omega)$. To express the remaining F's in terms of this one, a function $\varphi(\omega)$ is defined as

$$\varphi(\omega) = \frac{\omega}{P(\omega;M^2,m^2)}\;\frac{\Gamma(\omega)}{(\omega^2-\omega_o^2)^2 + \omega_o^2\Gamma^2(\omega)},$$

where ω_o is the central value of the resonance mass and

$$\Gamma(\omega) = \Gamma_o\left\{\frac{P(\omega;M^2,m^2)}{P(\omega_o;M^2,m^2)}\right\}^3\left[\frac{Am^2 + \{P(\omega_o;M^2,m^2)\}^2}{Am^2 + \{P(\omega;M^2,m^2)\}^2}\right]. \qquad (9)$$

Equation 9 expresses the P-wave energy-dependent width for two-body decays (appropriate for the P-wave resonance Δ^{++}). The quantity in square brackets is an empirical correction factor. The form of this factor is from nuclear reactions theory, and the value 2.2 for A is from a phase shift fit by Anderson as presented by Jackson (26). Physically, $(Am^2)^{-\frac{1}{2}}$ is the radius of interaction of the $p\pi^+$ (or $\bar{p}\pi^-$) system. Γ_o is the width parameter, with Anderson's fit resulting in the value 123 MeV.[1] The resulting ex-

[1] Jackson notes that Gell-Mann and Watson choose A = 1.3 and Γ_o = 116 MeV. In the present study, this value of A improved the fit slightly, but a larger width was preferred.

pression $F(\bar{\Delta}p\pi^+)$ [$F(\bar{p}\pi^-\Delta)$] is the three-body phase-space for production of the $\bar{\Delta}p\pi^+$ [$\bar{p}\pi^-\Delta$] final state multiplied by a Breit-Wigner distribution for the decay of the resonance. This is the probability that the three-body final state will be produced followed by the decay of the resonance, the resulting $\bar{p}\pi^-$ [$p\pi^+$] invariant mass being $\bar{\omega}$[ω]. Similarly, $F(\bar{\Delta}\Delta)$ is the two-body phase-space for the production of $\bar{\Delta}\Delta$ multiplied by Breit-Wigner expressions for the decay of each resonance. These forms assume the resonance production is "clean", i.e., interference effects are ignored.

The invariant mass distributions of Figure 9 were fitted to Expression 8 by maximum liklihood calculations. The constants C were evaluated by normalizing each of the functions F to unity. This requires the fractions α to sum to one. Charge conjugation requires $\alpha(\bar{\Delta}p\pi^+)$ to equal $\alpha(\bar{p}\pi^-\Delta)$. In addition to the fractions α, ω_o and Γ_o were allowed to vary in the fitting, giving a total of four free parameters. Allowing ω_o and Γ_o to vary required that the normalization constants be recalculated for each variation of either of these parameters. The results of the fit are presented after the following discussion.

A similar fitting procedure was used by Alles-Borelli et al. (12) at 5.7 GeV/c. The calculations of the $p\pi^+$ and $\bar{p}\pi^-$ invariant mass distributions using the parameters of the fit were found to be good representations of their data. This is not the case for the 2.4 and 2.9 GeV/c data, however. Apparently the expressions used in the fit are not good this close to threshold. The calculated $p\pi^+$ and $\bar{p}\pi^-$ mass distributions using the parameters of the fit are peaked slightly below the peaks in the data. Similar

difficulties were noted at 2.7 GeV/c (27). The problem seems to be that the calculated distributions have relatively less events on the low mass side of the peak as compared to the data. No combination of zero, single, and double resonance production in Expression 8 can reproduce the data exactly. The best fit is obtained by assuming small amounts of zero resonance production along with the double resonance production and setting ω_o well below the resonance mass. This gives a good representation of the sides of the distribution, but the calculated peak is at a lower mass than the peak in the data.

The fit is particularly sensitive to the form of the energy-dependent width. It was found that a better fit could be obtained by adjusting the empirical correction factor A in the energy-dependent width of Expression 9. The resulting fits to the data at 2.4, 2.7, and 2.9 GeV/c were found to be quite sensitive to the parameter A. In all cases the fit resulted in A being close to (but not equal to) zero. The effect of moving A from 2.2 to smaller values is to broaden the calculated distributions on the low mass side of the peak, leaving the high mass side unchanged. With A close to zero (corresponding to a very long radius of interaction), a calculated distribution with nearly 100% double resonance production is a better representation of the data at each momentum than is the corresponding "best fit" with A fixed at 2.2.

In fitting the 2.4 GeV/c data, there is yet another difficulty besides the form of the theoretical distribution. The kinematics require that the $p\pi^+$ and $\bar{p}\pi^-$ invariant masses be in or very near the $\overline{\Delta^{++}}$ Δ^{++} region. Consequently, zero and single resonance production can contribute only to this

region. This results in the fit to the theoretical distribution of Expression 8 being rather insensitive to the fractions of zero, single, and double resonance production.

Because of all of these uncertainties it was decided that "best estimates" of the parameters should be given along with the fitted values. These estimates were based in part on the above discussion of the fitting. Also considered were plots of the $p\pi^-$ and $p\pi^+$ invariant mass distributions for events in various Δ^2 bins. It is shown in Part C of this section that there is strong Δ^2 dependence in the interaction. Events which do not involve double resonance production might be found by examination of these mass distributions as functions of Δ^2. The scatter plots of the $p\pi^-$ versus the $p\pi^+$ invariant mass distributions binned on Δ^2 show very pronounced clustering of the events in the $\overline{\Delta^{++}}\ \Delta^{++}$ region at small Δ^2. This clustering becomes less pronounced with increasing Δ^2, due, at least in part, to kinematic effects. From these scatter plots it is clear that double resonance production accounts for nearly 100% of the events at small Δ^2, but it is difficult to make a conclusion concerning the amount of non-resonant background at large Δ^2. Calculations using the one-pion-exchange model (Section V) indicate, however, that even the events at large Δ^2 are consistent with nearly 100% $\overline{\Delta^{++}}\ \Delta^{++}$ production at both momenta. Also, the model calculations, based on double resonance production alone, predict cross-sections for Reaction 1 even greater than the measured values at both 2.4 and 2.9 GeV/c.

The best estimates based on these considerations are that the double resonance production is nearly 100% at both 2.4 and 2.9 GeV/c, any background being entirely non-resonant. The estimated resonance masses are the

values which give peaks in the calculated distributions corresponding to the peaks in the data. These estimates are shown along with the results of the four-parameter fits in Table 4. The errors quoted for the fitted values are purely statistical and do not reflect uncertainties in the forms used for the functions F.

Table 4. Fractions of zero, single, and double resonance production and the associated mass and width.

	2.4		2.9 GeV/c	
	Fitted Value	Best Estimate	Fitted Value	Best Estimate
$\alpha(\bar{p}\pi^- p\pi^+)$	0.17 ± 0.04	0.10 ± 0.10	0.06 ± 0.01	0.05 ± 0.05
$\alpha(\bar{\Delta}p\pi^+) = \alpha(\bar{p}\pi^- \Delta)$	0.00 ± 0.01	0.00 ± 0.05	0.00 ± 0.02	0.00 ± 0.02
$\alpha(\bar{\Delta}\Delta)$	0.83 ± 0.04	0.90 ± 0.10	0.94 ± 0.02	0.95 ± 0.05
ω_o (MeV)	128 ± 7	120 ± 8	126 ± 3	120 ± 8
Γ_o (MeV)	1213 ± 2	1221 ± 8	1220 ± 1	1231 ± 8

In contrast to the resonance production shown in Figure 9, there is no evidence for $\bar{\Delta}^0$ (1236) or Δ^0 (1236) in the $\bar{p}\pi^+$ and $p\pi^-$ invariant mass distributions of Figure 10. The distributions are smooth, and there is no clustering in the scatter plots. All other invariant mass distributions were also examined, and no evidence for resonance production was seen in any of them (as would be expected for the case of 100% $\bar{\Delta}^{++}$ Δ^{++} production). The $\pi^-\pi^+$ and $\bar{p}p$ distributions are shown in Figure 11. No known resonances decaying to $\pi^+\pi^-$ are energetically possible at 2.4 GeV/c and $\rho(765)$ is too close to the kinematic limit to be seen in the 2.9 GeV/c data. The bumps

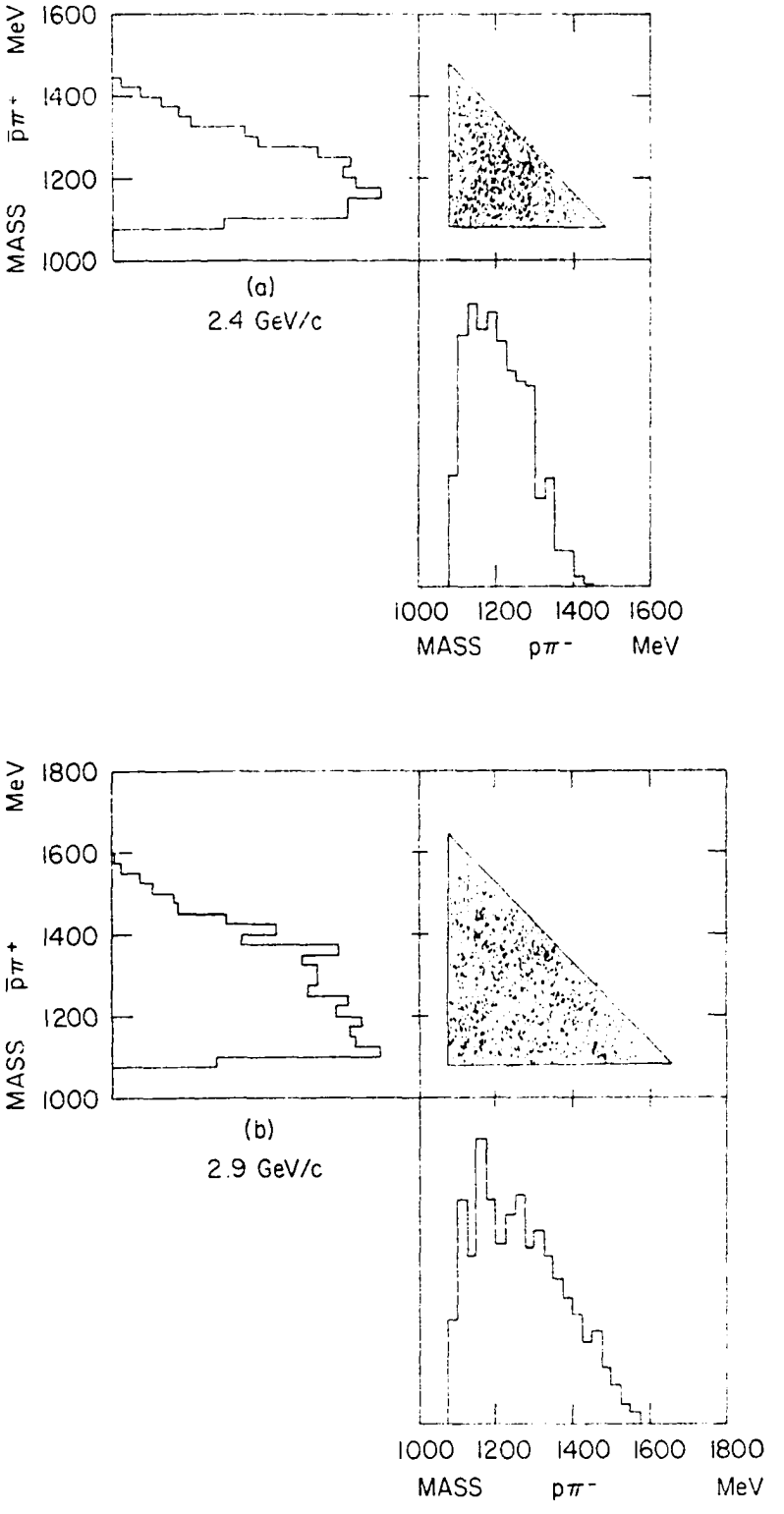

Figure 10. Scatter plots of the $p\pi^-$ versus the $\bar{p}\pi^+$ invariant mass distributions. The kinematic limits are indicated by the solid lines.

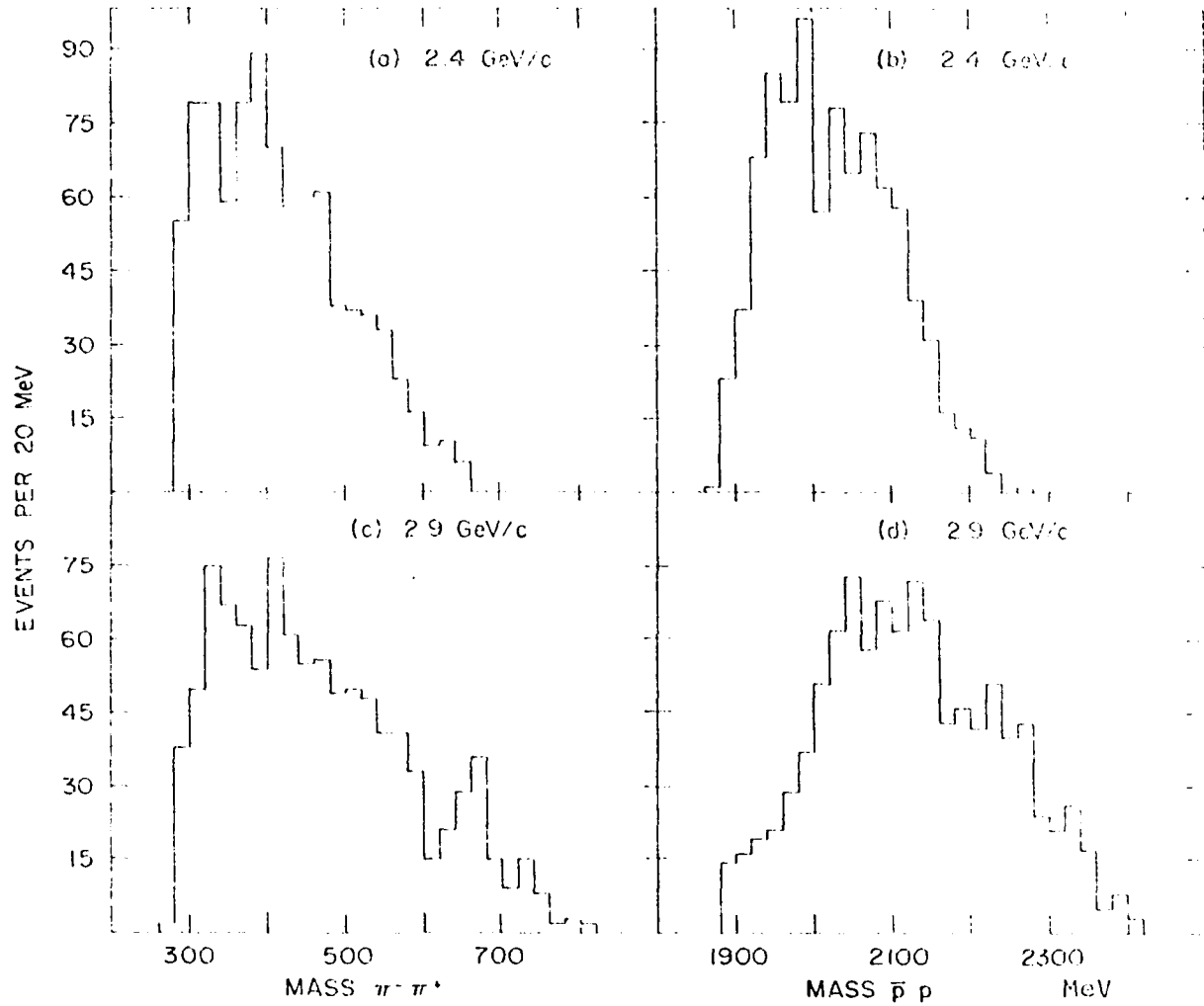

Figure 11. a), c) The invariant mass distributions of the $\pi^-\pi^+$ combination.
b), d) The invariant mass distributions for the $\bar{p}p$ combination.

appearing in these distributions are all apparently statistical fluctuations. No resonances are expected in the $\bar{p}p$ distribution, and none are seen. The $\bar{p}p\pi^-$ and $\bar{p}p\pi^+$ invariant mass distributions are shown in Figure 12. Again no resonances are expected or observed. Discussion of the $\bar{p}\pi^+\pi^-$ and $p\pi^+\pi^-$ invariant mass distributions is given in Section V, where they are shown combined at each momentum (they are identical within statistics at each momentum and charge conjugation invariance is invoked). Known resonances can occur in these distributions, and effects were reported by Bacon et al. (3) at 2.8 GeV/c. However, the conclusion of the present study is that the $\bar{p}\pi^+\pi^-$ and $p\pi^+\pi^-$ invariant mass distributions are adequately explained by the assumption of 100% $\overline{\Delta^{++}}\,\Delta^{++}$ production (at least at 2.7 and 2.9 GeV/c) and that no resonances occur in these distributions (see Section V).

B. Production Angular Distributions

In the remainder of this report, the results of Part A are considered to be consistent with 100% $\overline{\Delta^{++}}\,\Delta^{++}$ double resonance production (Reaction 2) at both 2.4 and 2.9 GeV/c. Comments are made at appropriate points to indicate the effects of adding a small non-resonant background. In studying such resonance production, it is customary to investigate the mechanism of production by examining the production angular distribution. The production angle θ_p is defined as the angle between the incident $\bar{p}$ momentum and the momentum of the outgoing $\overline{\Delta^{++}}$ (i.e., the $\bar{p}\pi^-$ system) in the center-of-mass. These distributions for the two momenta are shown in Figure 13. The reaction is seen to be peripheral at 2.4 GeV/c, with 38% of the events having $\cos\theta_p > 0.8$, and more strongly peripheral at 2.9 GeV/c, with 56% of the

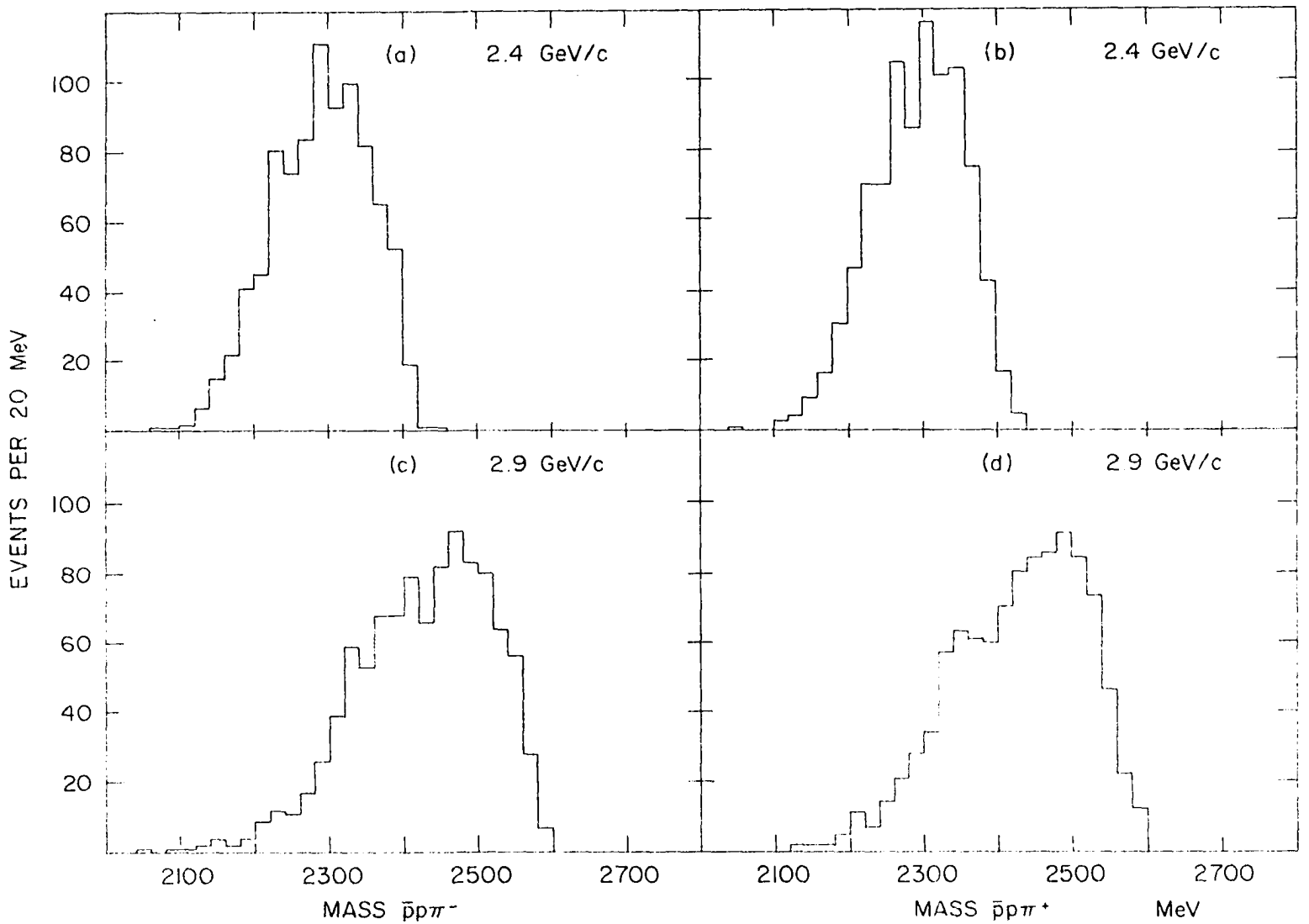

Figure 12. a), c) The invariant mass distributions of the $\bar{p}p\pi^-$ combination.
b), d) The invariant mass distributions for the $\bar{p}p\pi^+$ combination.

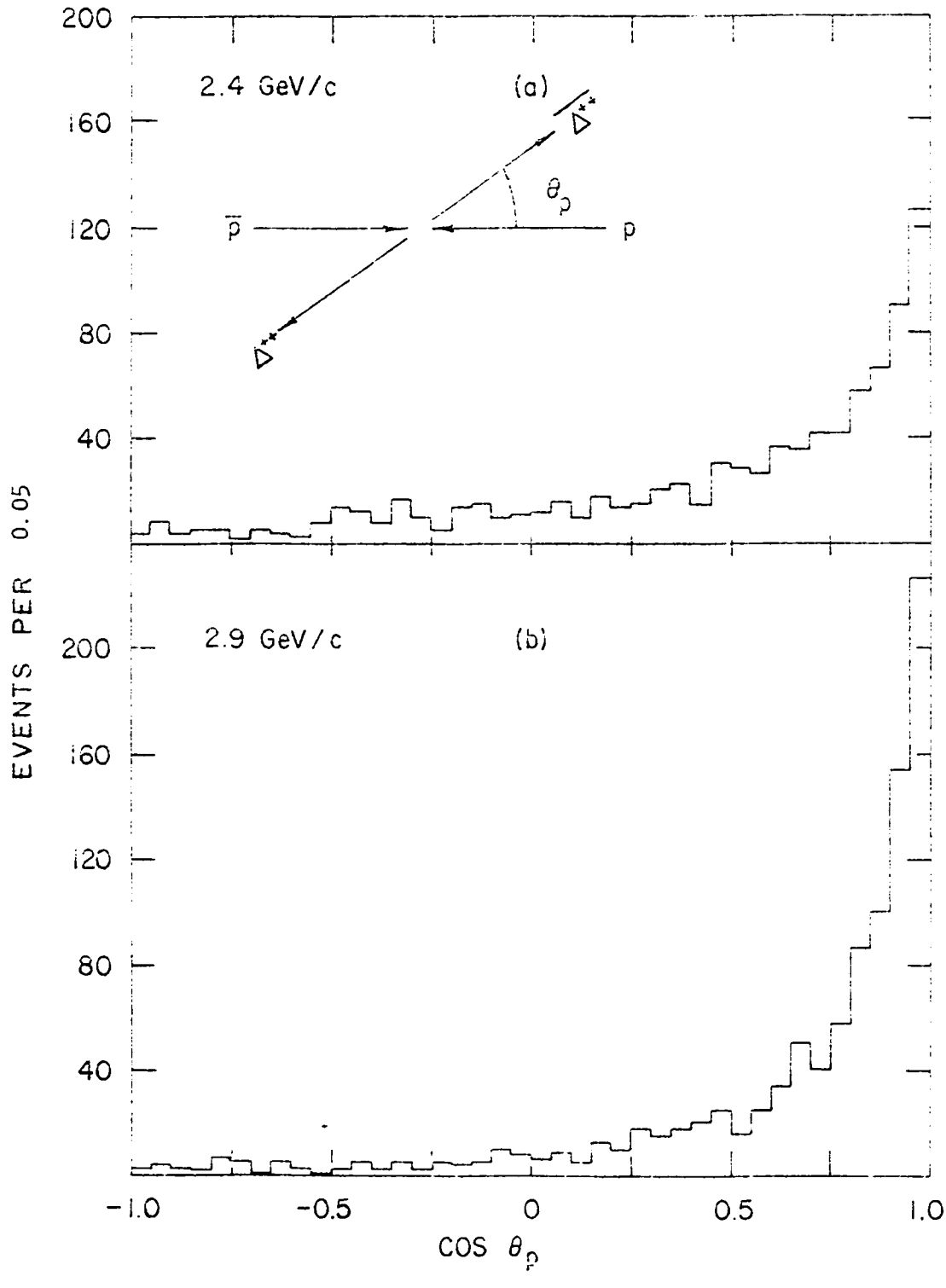

Figure 13. The center-of-mass production angular distributions.

events having $\cos\theta_p > 0.8$. Previous experiments concerning this and other quasi-two-body interactions have shown this tendency of the forward peak to become narrower with increasing beam momentum (28). An interpretation of the peripheral character of the reaction is given in Section V.

C. Decay Angular Distributions and Density Matrix Elements

Another aspect of the investigation of resonances is the examination of the angular distributions of decay. The angles are defined in Figure 14, where θ is the angle between the incident $\bar{p}(p)$ and the outgoing $\bar{p}(p)$ in the $\overline{\Delta^{++}}$ (Δ^{++}) rest frame, and ϕ is the corresponding azimuthal angle. The general form of the angular distribution of the $\overline{\Delta^{++}}(\Delta^{++})$ decay products in the $\overline{\Delta^{++}}$ (Δ^{++}) rest frame can be written in a model independent manner as (29)

$$W(\cos\theta,\phi) = C[(\tfrac{1}{2} - \rho_{1,1})\sin^2\theta + \rho_{1,1}(\tfrac{1}{3} + \cos^2\theta) - (2/\sqrt{3})\,\mathrm{Re}\rho_{3,-1}\sin^2\theta\cos2\phi - (2/\sqrt{3})\,\mathrm{Re}\rho_{3,1}\sin2\theta\cos\phi], \quad (10)$$

where C is a normalization constant. The ρ's are density matrix elements, with $\rho_{m,n}$ being the product of amplitudes for producing the Δ with spin projections m/2 and n/2 along the z axis in Figure 14. In other words, the density matrix gives the probabilities of the Δ having various spin orientations before its decay.

The individual $\cos\theta$ and ϕ distributions are obtained from Expression 10 by integration over ϕ and $\cos\theta$, respectively:

$$W_1(\cos\theta) = C_1[(\tfrac{3}{4} - \rho_{1,1}) + 3(\rho_{1,1} - \tfrac{1}{4})\cos^2\theta] \quad (11)$$

$$W_2(\phi) = C_2[(1 - 4/\sqrt{3})\,\mathrm{Re}\,\rho_{3,-1}\cos2\phi], \quad (12)$$

where C_1 and C_2 are normalization constants. By multiplying these expres-

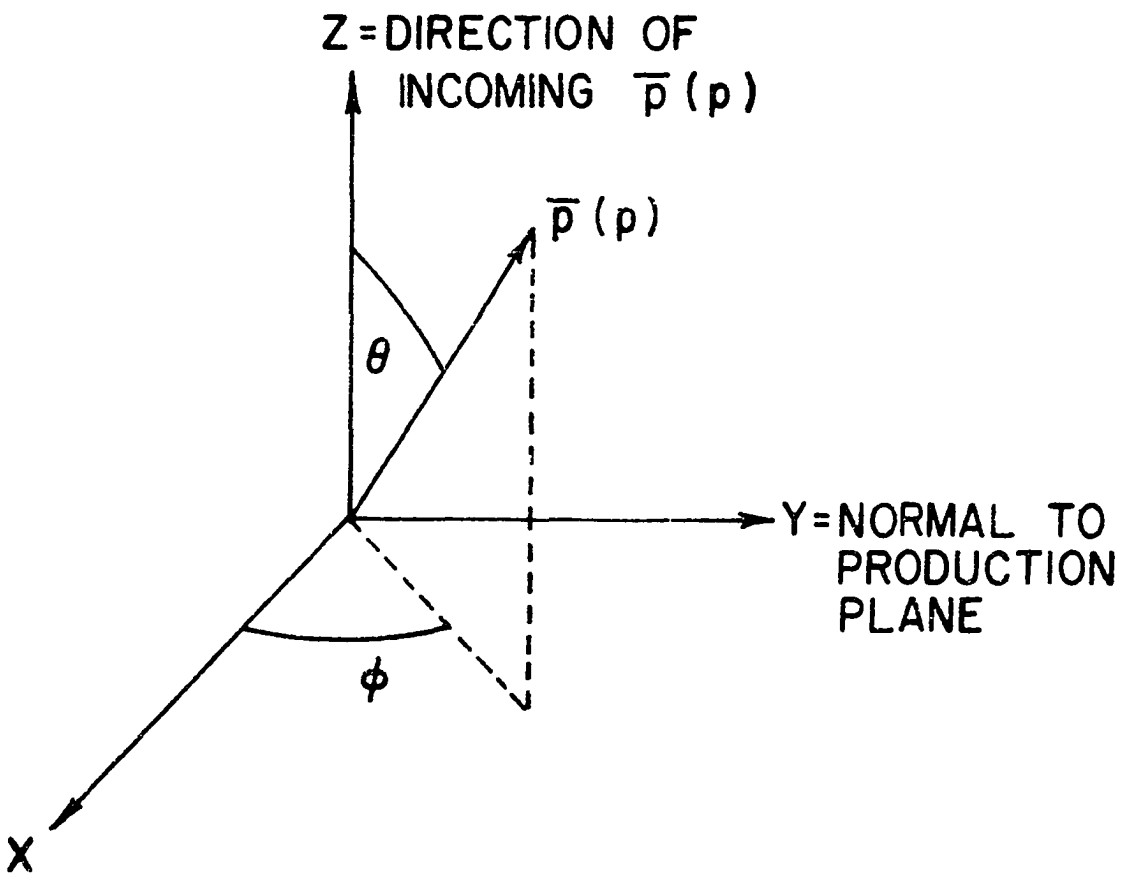

Figure 14. Definitions of the decay angles $\bar{\theta}$, $\bar{q}$ (θ, ϕ) in the $\bar{\Delta}^{--}$ (Δ^{++}) rest frame.

sions by various trigonometric functions of θ and ϕ and integrating, it is possible to find the following expressions:

$$\rho_{1,1} = \frac{15}{8}\langle\cos^2\theta\rangle - \frac{3}{8} \tag{13a}$$

$$\mathrm{Re}\rho_{3,1} = -\frac{5\sqrt{3}}{8}\langle\sin 2\theta \cos 2\phi\rangle \tag{13b}$$

$$\mathrm{Re}\rho_{3,-1} = -\frac{\sqrt{3}}{2}\langle\cos 2\phi\rangle. \tag{13c}$$

Here $\langle f(\cos\theta,\phi)\rangle$ denotes the average value of the function f, defined by

$$\langle f(\cos\theta,\phi)\rangle = \int_{-1}^{1} d(\cos\theta) \int_{0}^{\pi} d\phi\, W(\cos\theta,\phi)\, f(\cos\theta,\phi).$$

This quantity is determined from the data by

$$\langle f(\cos\theta,\phi)\rangle = \frac{1}{N}\sum_{i=1}^{N} f(\cos\theta,\phi),$$

where N is the number of events. The density matrix elements were calculated from Expression 13 by inserting the average values of the trigonometric functions determined from the data for the $\overline{\Delta^{++}}$ and Δ^{++} decays combined (charge conjugation invoked). The results are shown in Table 5 along with the predictions of the one-pion-exchange model, which is discussed in Section V. Inserting these values into Expressions 11 and 12 gave the "best fits" to the data shown in Figure 15. The fits to the $\cos\theta$ distributions are reasonably good, except for a tendency of the data at both 2.4 and 2.9 GeV/c to have more events near $\cos\theta = 1$ than near $\cos\theta = -1$. The fits to the ϕ distributions are not very good at either momentum. There are departures from isotropy, particularly at 2.4 GeV/c, but the calculation does not reproduce them very well. Further discussion of these distributions is given in Section V, where the model predictions shown in

Table 5. Independent spin-density matrix elements[a]

	2.4	2.7	2.9 GeV/c	OPE Model Prediction	Agreement
$\rho_{1,1}$	0.323 ± 0.013	0.348 ± 0.015	0.308 ± 0.013	0.5	bad
$\mathrm{Re}\rho_{3,1}$	-0.033 ± 0.014	-0.002 ± 0.015	-0.026 ± 0.012	0.0	fair
$\mathrm{Re}\rho_{3,-1}$	-0.028 ± 0.014	-0.038 ± 0.016	-0.026 ± 0.014	0.0	fair

[a]The values from the 2.7 GeV/c data are included here because of an error in the report of Crawley et al. (2).

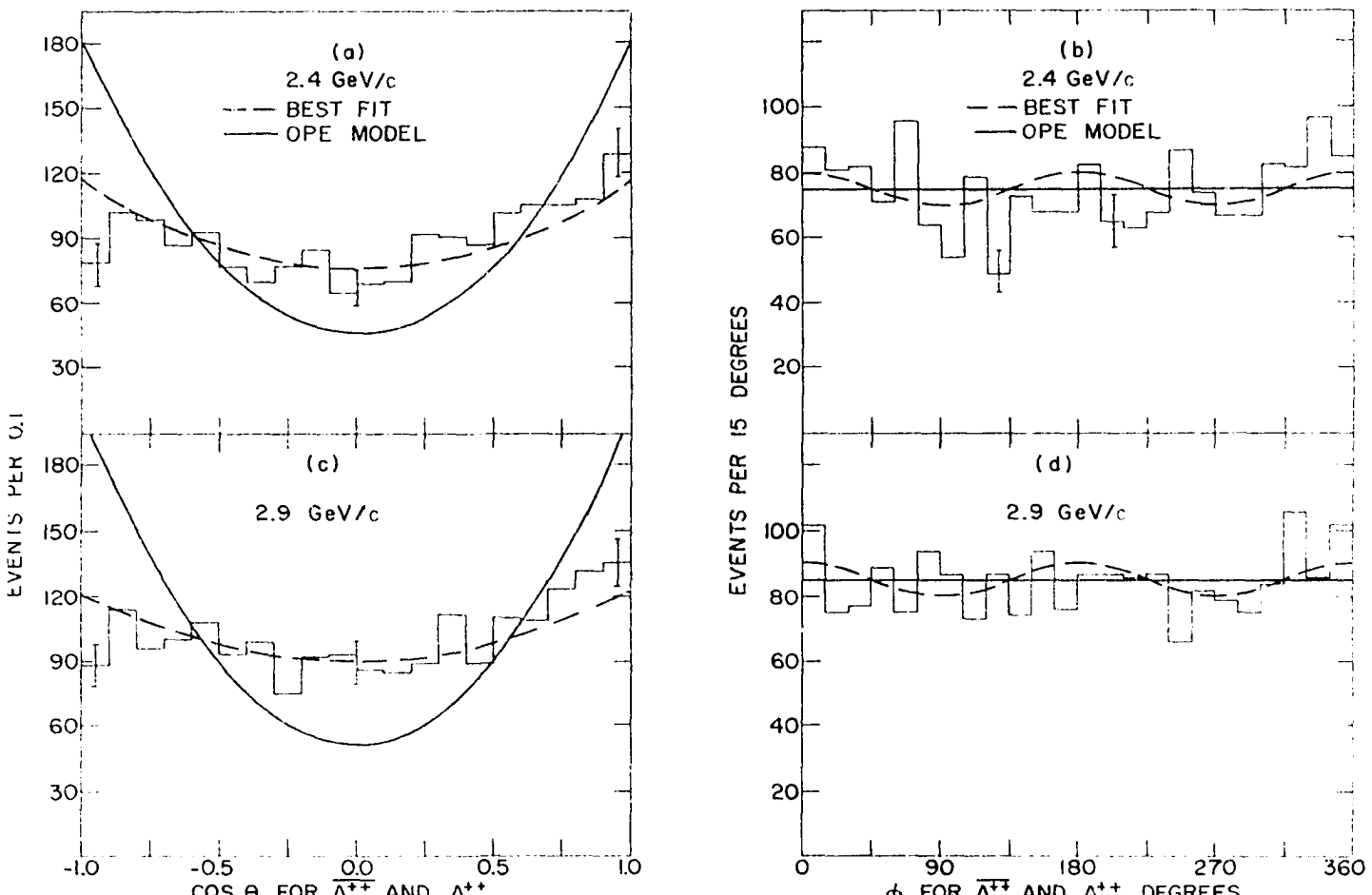

Figure 5. a), c) The cosθ distributions. b), d) The ϕ distributions. The angles are defined in Figure 14. The predictions of the OPE model and the best fit are also shown.

Figure 15 are presented.

Pilkuhn and Svensson (30) have pointed out that still more information about the decays can be found by examining the joint decay distribution $W(\cos\bar{\theta}, \cos\theta, \bar{\phi}, \phi)$, where $\bar{\theta}$, $\bar{\phi}$ (θ, ϕ) are the decay angles of the $\bar{\Delta}^{++}$ (Δ^{++}). This allows the determination of thirteen additional independent production amplitudes (but not the complete density matrix), which have been evaluated by Alles-Borelli et al. (12) using the method described above for the independent density matrix elements.[1] The expressions are

$$\frac{1}{2}(\rho^{3,3} - \rho^{1,1}) = \frac{25}{16}\langle(1-3\cos^2\bar{\theta})(1-3\cos^2\theta)\rangle \tag{14a}$$

$$\mathrm{Re}\rho^{3,1} = -\frac{25\sqrt{3}}{16}\langle(1-3\cos^2\theta)\sin2\bar{\theta}\cos\bar{\phi}\rangle \tag{14b}$$

$$\mathrm{Re}\overline{\rho_{3,1}} = -\frac{25\sqrt{3}}{16}\langle(1-3\cos^2\bar{\theta})\sin2\theta\cos\phi\rangle \tag{14c}$$

$$\mathrm{Re}\rho^{3,-1} = -\frac{5\sqrt{3}}{4}\langle(1-3\cos^2\theta)\cos2\bar{\phi}\rangle \tag{14d}$$

$$\mathrm{Re}\overline{\rho_{3,-1}} = -\frac{5\sqrt{3}}{4}\langle(1-3\cos^2\bar{\theta})\cos2\phi\rangle \tag{14e}$$

$$\mathrm{Re}(\rho^{3,1}_{3,1} - \rho^{-1,-3}_{3,1}) = \frac{225}{96}\langle\sin2\bar{\theta}\sin2\theta\cos(\bar{\phi}+\phi)\rangle \tag{14f}$$

$$\mathrm{Re}(\rho^{3,1}_{1,3} - \rho^{-1,-3}_{1,3}) = \frac{225}{96}\langle\sin2\bar{\theta}\sin2\theta\cos(\bar{\phi}-\phi)\rangle \tag{14g}$$

$$\mathrm{Re}(\rho^{3,-1}_{3,1} + \rho^{1,-3}_{3,1}) = \frac{15}{8}\langle\sin2\theta\cos(2\bar{\phi}+\phi)\rangle \tag{14h}$$

$$\mathrm{Re}(\rho^{3,-1}_{1,3} + \rho^{1,-3}_{1,3}) = \frac{15}{8}\langle\sin2\theta\cos(2\bar{\phi}-\phi)\rangle \tag{14i}$$

$$\mathrm{Re}(\rho^{3,1}_{3,-1} - \rho^{-1,-3}_{3,-1}) = \frac{15}{8}\langle\sin2\bar{\theta}\cos(\bar{\phi}+2\phi)\rangle \tag{14j}$$

---

[1] There are a number of errors in the expressions of Reference 12. The forms given here were calculated by R. A. Leacock.

$$\mathrm{Re}(\rho^{3,1}_{-1,3} - \rho^{-1,-3}_{-1,3}) = \frac{15}{8} \langle \sin 2\bar{\theta} \cos(\bar{\Phi} - 2\Phi) \rangle \tag{14k}$$

$$\mathrm{Re}(\rho^{3,-1}_{3,-1} + \rho^{1,-3}_{3,-1}) = \frac{3}{2} \langle \cos 2(\bar{\Phi} + \Phi) \rangle \tag{14ℓ}$$

$$\mathrm{Re}(\rho^{3,-1}_{-1,3} + \rho^{1,-3}_{-1,3}) = \frac{3}{2} \langle \cos 2(\bar{\Phi} - \Phi) \rangle \tag{14m}$$

where

$$\underline{\rho}^{m,n} = \rho^{m,n}_{3,3} + \rho^{m,n}_{-3,-3} - \rho^{m,n}_{1,1} - \rho^{m,n}_{-1,-1} \tag{15a}$$

$$\overline{\rho}^{m,n} = \rho^{3,3}_{m,n} + \rho^{-3,-3}_{m,n} - \rho^{1,1}_{m,n} - \rho^{-1,-1}_{m,n} \; . \tag{15b}$$

The values obtained from the data are given in Table 6, where they are compared to the predictions of the one-pion-exchange model (discussed in Section V).

These matrix elements were also calculated as functions of Δ^2, the square of the four-momentum transferred from the incident $\bar{p}$ to the outgoing $\bar{p}\pi^-$ system. This was done by applying the method described above to the data in various Δ^2 bins. The results are shown in Figure 16, and are discussed in Sections V and VI.

Table 6. Joint spin-density matrix elements[a]

	2.4	2.7	2.9 GeV/c	OPE Model Prediction	Agreement
$\frac{1}{2}(\underline{\rho}^{3,3} - \underline{\rho}^{1,1})$	0.052 ± 0.045	0.033 ± 0.050	0.086 ± 0.042	0.25	bad
$\mathrm{Re}\underline{\rho}^{3,1}$	-0.002 ± 0.045	0.014 ± 0.052	0.004 ± 0.040	0.0	good
$\mathrm{Re}\overline{\rho}_{3,1}$	0.034 ± 0.045	-0.010 ± 0.051	0.020 ± 0.043	0.0	good
$\mathrm{Re}\underline{\rho}^{3,-1}$	0.048 ± 0.048	0.063 ± 0.054	0.022 ± 0.043	0.0	fair
$\mathrm{Re}\overline{\rho}_{3,-1}$	0.107 ± 0.046	0.000 ± 0.052	-0.020 ± 0.044	0.0	fair
$\mathrm{Re}(\rho^{3,1}_{3,1} - \rho^{-1,-3}_{3,1})$	-0.010 ± 0.031	-0.019 ± 0.036	-0.053 ± 0.029	0.0	fair
$\mathrm{Re}(\rho^{3,1}_{1,3} - \rho^{-1,-3}_{1,3})$	0.030 ± 0.031	0.017 ± 0.035	0.019 ± 0.028	0.0	good
$\mathrm{Re}(\rho^{3,-1}_{3,1} + \rho^{1,-3}_{3,1})$	0.028 ± 0.033	0.040 ± 0.038	0.079 ± 0.031	0.0	fair
$\mathrm{Re}(\rho^{3,-1}_{1,3} + \rho^{1,-3}_{1,3})$	-0.004 ± 0.032	0.039 ± 0.036	0.027 ± 0.032	0.0	fair

[a]The values from the 2.7 GeV/c data of Crawley *et al.* (2) are present here because they were not previously calculated.

Table 6 (Continued).

	2.4	2.7	2.9 GeV/c	OPE Model Prediction	Agreement
$Re(\rho^{3,1}_{3,-1} - \rho^{-1,-3}_{3,-1})$	0.018 ± 0.034	0.035 ± 0.037	0.007 ± 0.030	0.0	good
$Re(\rho^{3,1}_{-1,3} - \rho^{-1,-3}_{-1,3})$	-0.026 ± 0.033	0.089 ± 0.037	0.000 ± 0.031	0.0	fair
$Re(\rho^{3,-1}_{3,-1} + \rho^{1,-3}_{3,-1})$	0.004 ± 0.035	0.062 ± 0.040	0.038 ± 0.033	0.0	fair
$Re(\rho^{3,-1}_{-1,3} + \rho^{1,-3}_{-1,3})$	-0.016 ± 0.035	-0.010 ± 0.039	-0.026 ± 0.034	0.0	good

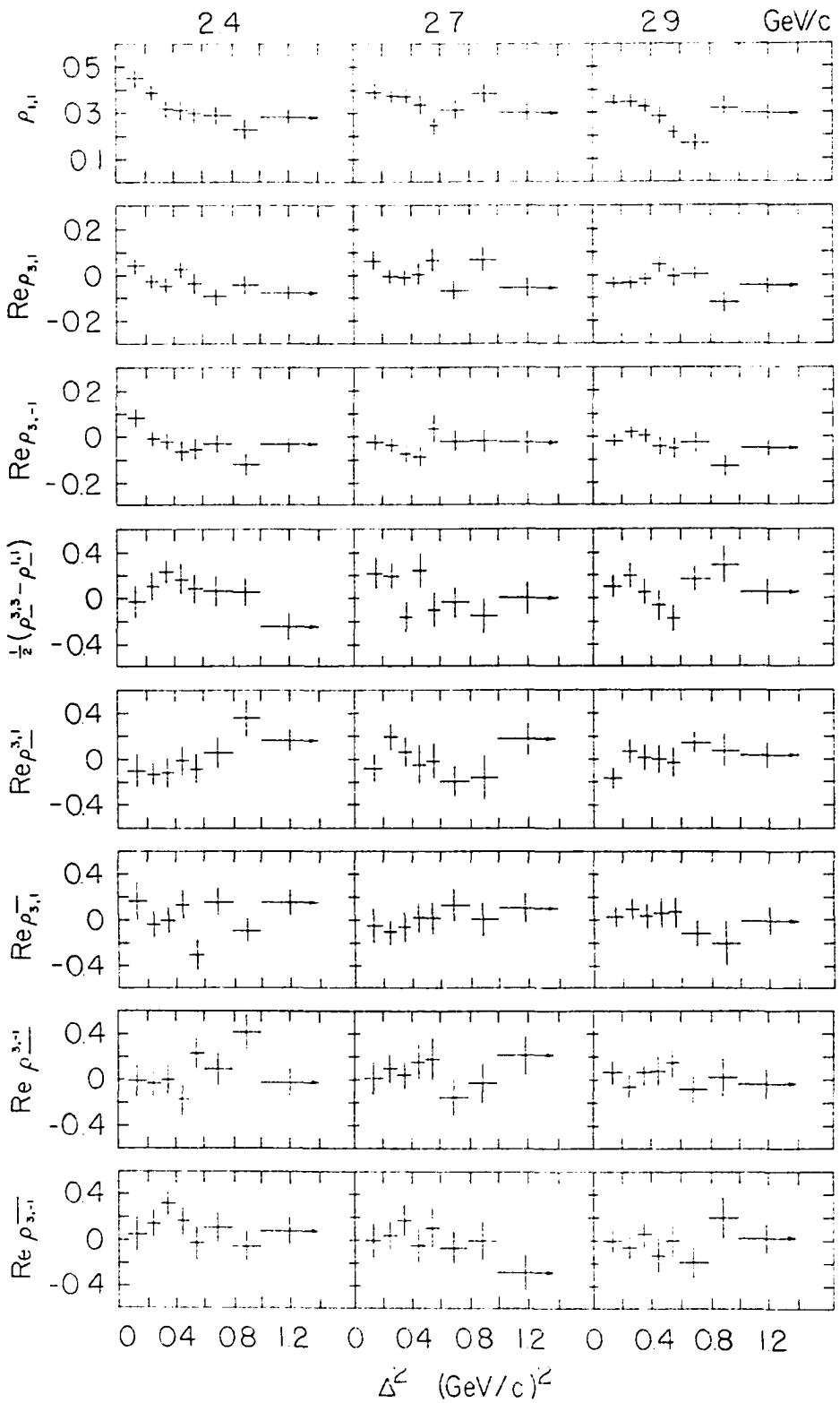

Figure 16a. The spin-density matrix elements as functions of Δ^2.

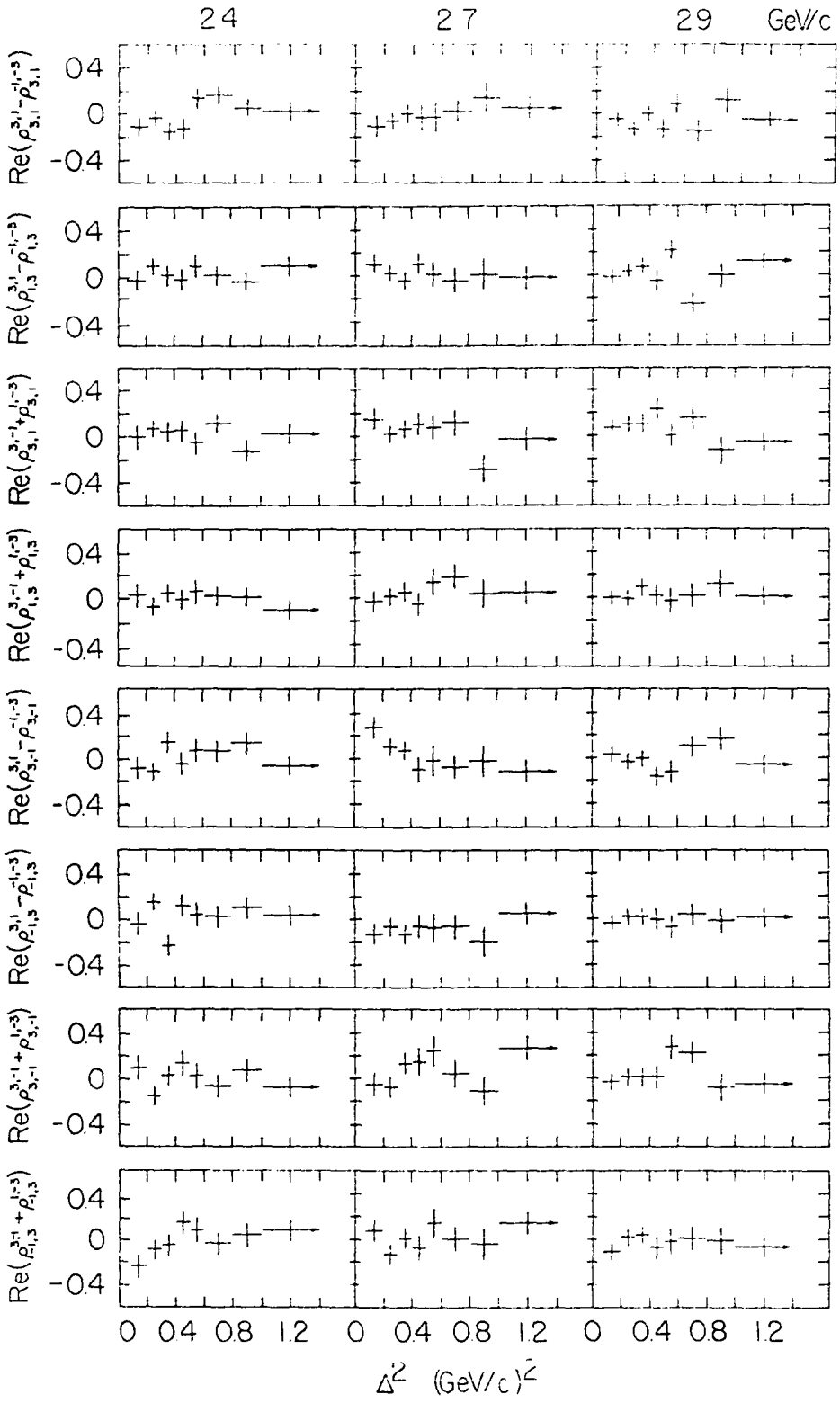

Figure 16b. The spin-density matrix elements as functions of Δ^2.

V. COMPARISON OF THE DATA WITH THE ONE-PION-EXCHANGE MODEL

It was noted in Section IV that Reaction 1 is peripheral, particularly at 2.9 GeV/c. This suggests the exchange of a light particle, the pi meson, in the interaction, and indicates the possibility of interpreting the data using the one-pion-exchange (OPE) model. In this section, the OPE calculations are discussed and compared to the data. The choice of Feynman diagrams to be used in the calculations is discussed in Part A. In Part B, the predictions for the spin-density matrix elements are given, while Part C is devoted to a discussion of the differential cross-section $d\sigma/(d\bar{\omega}^2\, d\omega^2\, d\Delta^2)$ and the resulting predictions of the $\bar{p}\pi^-$ (or $p\pi^+$) invariant mass distributions and the four-momentum transfer distributions. The total cross-section predictions and the calculations of the $\bar{p}\pi^+\pi^-$ (or $p\pi^+\pi^-$) invariant mass distributions are discussed and compared to the data in Parts D and E, respectively.

A. The Feynman Diagrams

All possible OPE diagrams for Reaction 1 are shown in Figure 17. The general form for the contribution of the double-isobar and $I_z = \frac{1}{2}$ diagrams to the differential cross-section is (15)

$$\frac{d\sigma}{d\bar{\omega}^2\, d\omega^2\, d\Delta^2} = \Omega\, f_\ell\, \sigma_\ell(\omega)\, \frac{1}{(\Delta^2+m^2)^2}\, f_u\, \sigma_u\, (\bar{\omega}), \qquad (16)$$

where f_ℓ and f_u are kinematical and dynamical factors for the lower and upper vertex, respectively, and σ_ℓ and σ_u are the corresponding cross-sections for the appropriate $N\pi$ scattering process at each vertex. Ω is a product of form-factors and off-shell corrections, and $(\Delta^2+m^2)^{-1}$ is the pion propagator. $\bar{\omega}(\omega)$ is the invariant mass of the outgoing particles

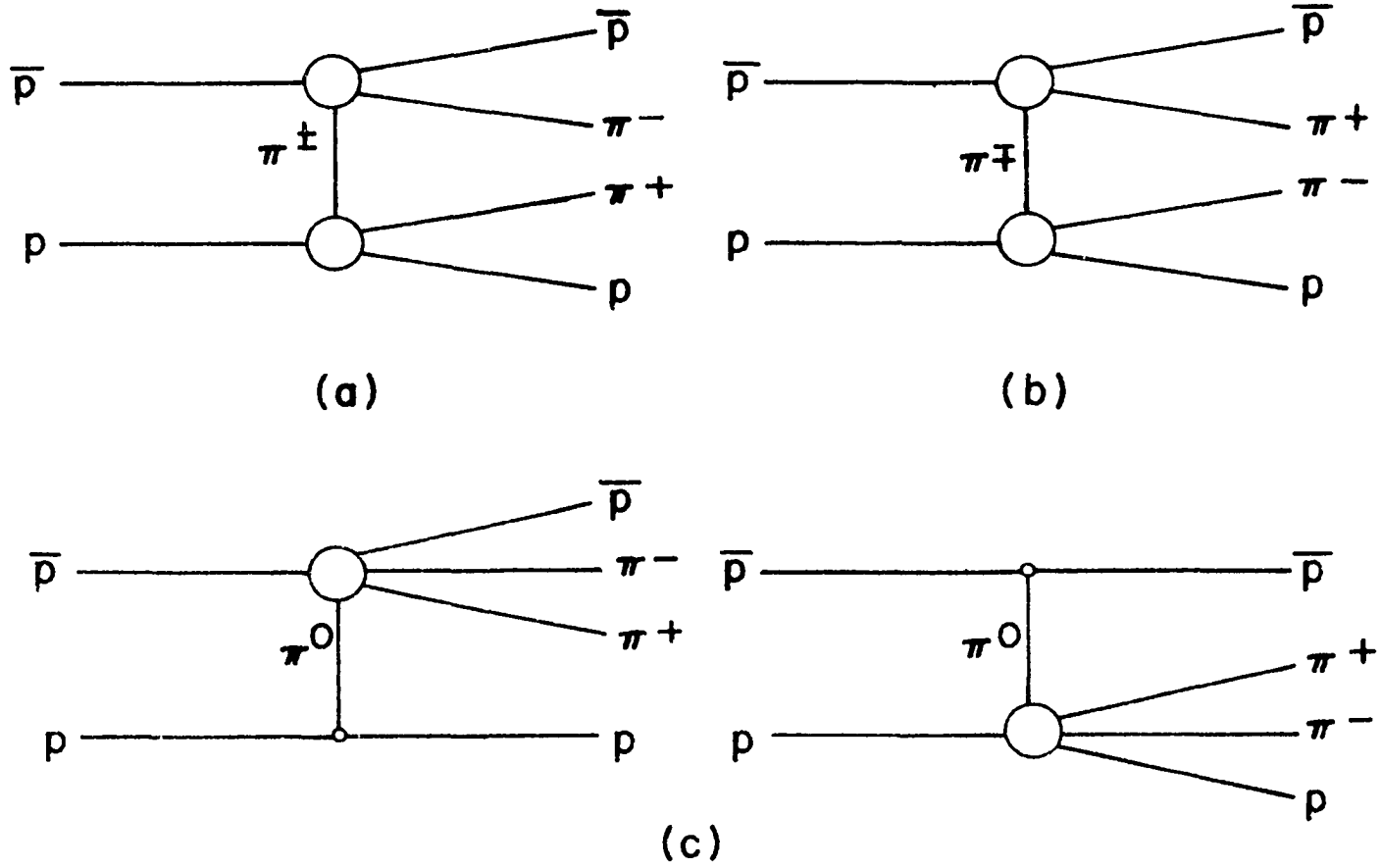

Figure 17. OPE diagrams for the reaction $\bar{p}p \to \bar{p}p\pi^+\pi^-$. a) Double-isobar diagram. b) $I_z = \frac{1}{2}$ diagram. c) Drell diagrams.

at the upper (lower) vertex, and Δ^2 is the square of the four-momentum transferred from the incoming nucleon to the outgoing system at the same vertex.

The principal difference between Expression 16 for the double-isobar diagram and the $I_z = \frac{1}{2}$ diagram is in the cross-section σ_ℓ (σ_u). For the double-isobar diagram, this is the cross-section for the elastic scattering process $\pi^+ p \to \pi^+ p$ ($\pi^- \bar{p} \to \pi^- \bar{p}$), while for the $I_z = \frac{1}{2}$ diagram the reaction is $\pi^- p \to \pi^- p$ ($\pi^+ \bar{p} \to \pi^+ \bar{p}$). The ratio of the former cross-section to the latter is 9:1, so the ratio of the predicted contribution to the differential cross-section in Expression 14 is 81:1. For this reason the $I_z = \frac{1}{2}$ diagram was neglected in the calculations.

The form for the contribution of the two Drell diagrams to the differential cross-section is given by Ferrari (31) as

$$\frac{d\sigma}{d\omega^2\, d\Delta^2} = \Lambda(\Delta^2)\, \frac{G^2}{4\pi W^2 P_{cm}^2}\, \frac{\Delta^2}{(\Delta^2+m^2)^2}\, P(\omega;M^2,m^2)\, \omega\, \sigma_o(\omega), \quad (17)$$

where the product of form-factors and off-shell corrections is

$$\Lambda(\Delta^2) = [1 + (\Delta^2+m^2)/90m^2]^{-2}$$

and where

$$P(\omega;M^2,m^2) = \frac{1}{2\omega}[\omega^4 - 2\omega^2(M^2 + m^2) + (M^2 - m^2)^2]^{1/2}.$$

$G^2 = 14.5$ is the NπN coupling constant, W is the total center-of-mass energy, and P_{cm} is the center-of-mass momentum. ω is the invariant mass of the final N$\pi\pi$ system, and Δ^2 is the square of the four-momentum transferred from the incoming nucleon to that system at the same vertex. $\sigma_o(\omega)$ is the cross-section for the reaction $\pi^- p \to \pi^+ \pi^- p$ (or $\pi^- \bar{p} \to \pi^- \pi^+ \bar{p}$), which cannot be observed directly. Estimates of this cross-section have

been made by Ferrari (31) using isotopic spin arguments and the observed cross-sections for other $\pi N \rightarrow \pi\pi N$ reactions. His result was represented by a second order polynomial in ω, and Equation 17 was integrated over the allowed values of Δ^2 and ω to determine the expected contribution of the Drell diagrams to the Reaction 1 cross-section at each momentum. The values obtained are 0.6 mb at 2.4 GeV/c and 1.3 mb at 2.9 GeV/c. These values are 40% and 51%, respectively, of the cross-sections for Reaction 1 reported in Section III. However, the Drell diagrams can contribute only to zero or single resonance production. Since the conclusion of Section IV was that the reaction proceeds almost entirely through double resonance production, the Drell diagrams were neglected on empirical grounds. Also neglected were possible contributions from rho meson exchange. These contributions are expected to be small compared to those for pion exchange due to the larger mass in the rho propagator. The model calculations which follow are based entirely on the double-isobar one-pion-exchange diagram. It is shown in Part D that the calculated contribution to the Reaction 1 cross-section from this diagram alone is even larger than the measured cross-section at each momentum.

B. Spin-Density Matrix Elements

The one-pion-exchange model for Reaction 1, as based on the double-isobar diagram, assumes the exchange of a spinless particle and no final state interactions. The $N\pi$ relative orbital angular momentum is perpendicular to the z axis in Figure 14, so the only possible spin projections of the Δ along the z axis are $\pm \frac{1}{2}$. Thus the only non-zero elements expected in the independent density matrix are the ones for these projections,

namely $\rho_{1,1}$ and $\rho_{-1,-1}$. Since $\sum_m \rho_{m,m} = 1$ and $\rho_{m,m} = \rho_{-m,-m}$ (30), the predictions for the density matrix elements are $\rho_{1,1} = \frac{1}{2}$ and $Re\rho_{3,1} = Re\rho_{3,-1} = 0$. The experimental results of Table 5 disagree with this value of $\rho_{1,1}$ at all three momenta. An even more striking disagreement between the model and the data is the strong Δ^2 dependence of $\rho_{1,1}$ shown in Figure 16. A calculation by Svensson (32) taking into account absorption by other possible final states accounts for a comparable effect in the data at 3.6 and 5.7 GeV/c. However, a similar calculation by Hite and Jackson as presented by Crawley (2) failed to reproduce the effect at 2.7 GeV/c.

Using the model predictions for the density matrix elements in Expressions 11 and 12 results in the predicted distribution $W_1(\cos\theta)$ having the simple form $1 + 3\cos^2\theta$, while $W_2(\phi)$ is independent of the azimuthal angle ϕ. These forms are compared with the data in Figure 15. The agreement with the $\cos\theta$ distributions is seen to be very poor at both 2.4 and 2.9 GeV/c, and the ϕ distributions show deviations from isotropy, particularly at 2.4 GeV/c.

The above argument concerning the model predictions for the independent density matrix elements applies to the joint density matrix elements as well. So all elements having ± 3 in either the superscript or the subscript are predicted to be zero. This means that the only non-zero element expected among the terms in Expressions 14 is $\underline{\rho^{1,1}}$ in 14a. From Equation 15 and $\sum_{m,n} \rho^{m,m}_{n,n} = 1$ (30), the expected value is $\underline{\rho^{1,1}} = -\rho^{1,1}_{1,1} - \rho^{1,1}_{-1,-1} = -\frac{1}{2}$, or $\frac{1}{2}(\underline{\rho^{3,3}} - \underline{\rho^{1,1}}) = \frac{1}{4}$. The experimental value of this quantity shown in Table 6 does not agree with this prediction. This is

to be expected because of the relationship of $\underline{\rho^{1,1}}$ to $\rho_{1,1}$, which also differs from the prediction. All of the other joint density matrix elements in Table 6 are in reasonably good agreement with the model, indicating little or no correlation in the $\overline{\Delta^{++}}$ and Δ^{++} production. Some Δ^2 dependence in a few of these terms is indicated in Figure 16; however, most of these fluctuations are not statistically significant.

C. $\bar{p}\pi^-$ and $p\pi^+$ Invariant Mass and Δ^2 Distributions

The one-pion-exchange model predictions of the spin-density matrix elements do not depend on any form-factors which may be used to account for the virtuality of the exchanged pion and other off-shell effects. For calculations which do depend on these quantities, the form-factor of Dürr and Pilkuhn (17) as fitted by Wolf (28) was used. The differential cross-section for Reaction 1 is given by (2, 15)

$$\frac{d\sigma}{d\bar{\omega}^2\, d\omega^2\, d\Delta^2} = \Omega(\bar{\omega},\omega,\Delta^2)\frac{1}{16\pi^3 F^2}\ \omega P(\omega;M^2,m^2)\sigma_1(\omega) \times \frac{1}{(\Delta^2+m^2)^2}\ \bar{\omega}\, P(\bar{\omega};M^2,m^2)\sigma_1(\bar{\omega}), \tag{18}$$

where the notation is the same as that used in Part A. F^2 is a kinematical factor defined by $F^2 = (P_1 \cdot P_2)^2 - M^4$, where $P_1(P_2)$ is the incoming $\bar{p}(p)$ four-momentum. $\sigma_1(\bar{\omega})[\sigma_1(\omega)]$ is the total cross-section for the $\bar{p}\pi^- \to \bar{p}\pi^-[p\pi^+ \to p\pi^+]$ scattering process occurring at the upper [lower] vertex of the double-isobar diagram. For $\sigma_1(\omega)$, the Breit-Wigner form

$$\sigma_1(\omega) = \frac{2\pi}{[P(\omega;M^2,m^2)]^2}\ \frac{[\Gamma(\omega)]^2}{(\omega-\omega_o)^2 + [\frac{1}{2}\Gamma(\omega)]^2} \tag{19}$$

was used, with the empirically corrected energy-dependent width expression

of Gell-Mann and Watson (33):

$$\Gamma(\omega) = 2\gamma_\lambda^2 [P(\omega;M^2,m^2)a]^3/[1 + \{P(\omega;M^2,m^2)a\}^2] ,$$

where $2\gamma_\lambda^2$ = 116 MeV, a = 0.88/m, and ω_o = 1236 MeV are the parameters of a fit to the data. Although the fit was done several years ago, comparison of the calculated values of $\sigma_1(\omega)$ with a recent compilation of π^+p elastic scattering data (34) shows that the fit gives a good representation of the data. This form of $\Gamma(\omega)$ is equivalent to the form given in Section IV, where Γ_o and A correspond to $2\gamma_\lambda^2$ and $(am)^{-2}$, respectively (a = .88/m implies A = 1.3). $\Omega(\bar{\omega},\omega,\Delta^2)$is the over-all form factor (17, 28) defined by

$$\Omega(\bar{\omega},\omega,\Delta^2) = G^2(\Delta^2)\ \Lambda(\bar{\omega},\Delta^2)\Lambda(\omega,\Delta^2) ,$$

where

$$\Lambda(\omega,\Delta^2) = \frac{(\omega + M)^2 + \Delta^2}{(\omega + M)^2 - m^2} \left[\frac{P(\omega;M^2,-\Delta^2)}{P(\omega;M^2,m^2)}\right]^2 \frac{1 + R^2[P(\omega;M^2,m^2)]^2}{1 + R^2[P(\omega;M^2,-\Delta^2)]^2}$$

and $G(\Delta^2) = (c-m^2)/(c+\Delta^2)$. The empirical parameters determined by Wolf (28) from a fit to the data for several reactions are c = 2.29 ± 0.27 $(GeV)^2$ and R = 2.97 ± 0.11 $(GeV)^{-1}$.

Integration of Equation 18 over $\bar{\omega}^2$ and ω^2 results in the double-isobar one-pion-exchange model prediction of the differential cross-section with respect to Δ^2. This prediction at each momentum is shown normalized to the data in Figure 18. The agreement is seen to be very good at 2.9 GeV/c, even for large Δ^2. At 2.4 GeV/c, the calculated peak is slightly too broad, but is a reasonable representation of the data.

Integration of Equation 18 over Δ^2 and $\bar{\omega}^2$ results in the model prediction of the differential cross-section with respect to ω. This predic-

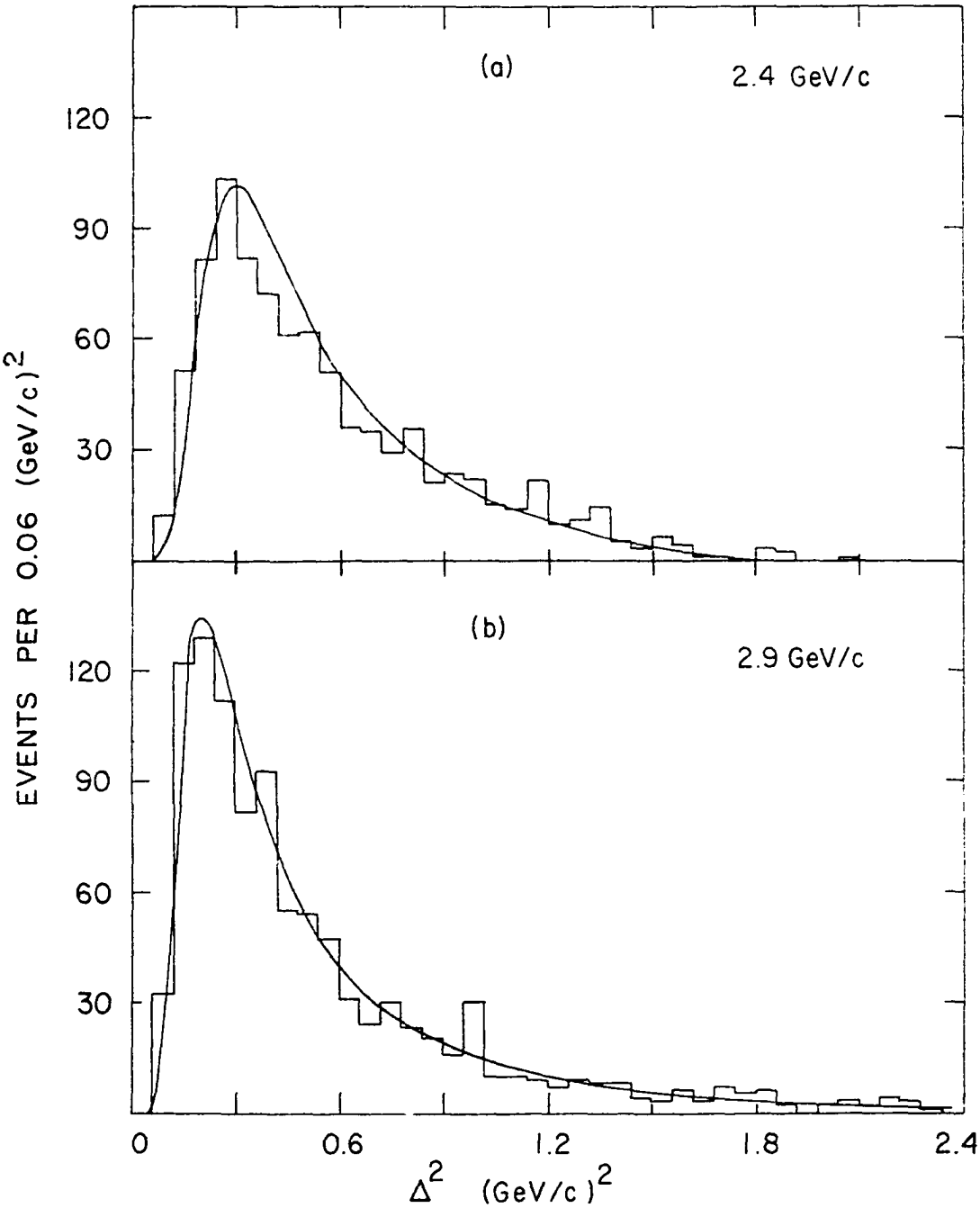

Figure 18. The Δ^2 distributions. The solid curves are the predictions of the double-isobar OPE model normalized to the data.

tion at each momentum is shown normalized to the combined $\bar{p}\pi^-$ and $p\pi^+$ invariant mass distributions in Figure 19. The shapes of the calculated peaks are seen to be good representations of the data, but they are centered at slightly higher mass than are the data, particularly at 2.4 GeV/c. The phase-space predictions for these distributions are considerably broader than the double-isobar curves and are peaked at somewhat lower mass. The predictions of the double-isobar model were also compared with the combined $\bar{p}\pi^-$ and $p\pi^+$ invariant mass distributions in various Δ^2 bins. The agreement was seen to be approximately the same for all Δ^2 at both momenta, supporting the conclusion of nearly 100% double resonance production.

D. Cross-Sections

The only dependence of these calculations on the data presented here is in the over-all normalization. An absolute prediction of the model is the total cross-section for $\bar{p}p \rightarrow \overline{\Delta^{++}}\,\Delta^{++}$. The predictions at 2.4, 2.7 and 2.9 GeV/c are 1.94, 2.60, and 2.82 mb, respectively, based on the double-isobar diagram alone. These are compared to the experimental cross-sections for Reaction 1 of 1.48 ± .07, 1.93 ± .16, and 2.53 ± .10 mb, respectively, at these momenta. It is seen that the energy dependence is roughly correct, but that the model predictions are too large by an over-all multiplicative constant (1.3 at 2.4 and 2.7 GeV/c, 1.1 at 2.9 GeV/c) in Expression 18. Comparison with other data is given in Section VI.

E. $\bar{p}\pi^+\pi^-$ and $p\pi^+\pi^-$ Invariant Mass Distributions

The double-isobar one-pion-exchange model also predicts the differen-

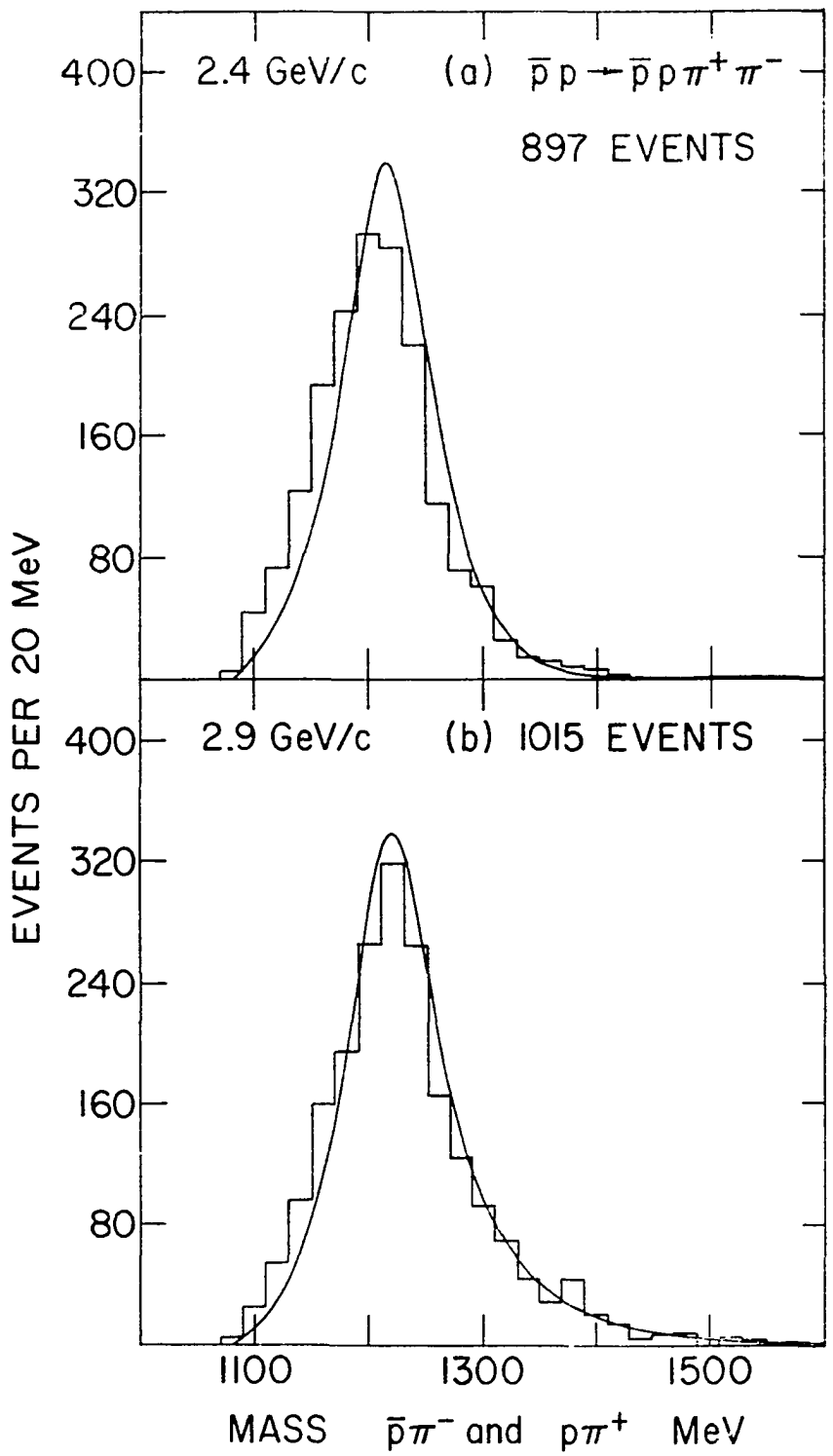

Figure 19. The $\bar{p}\pi^-$ and $p\pi^+$ invariant mass distributions combined. The solid curves are the predictions of the double-isobar OPE model normalized to the data.

tial cross-section with respect to u, the $p\pi^+\pi^-$ invariant mass. The $\bar{p}\pi^+\pi^-$ and $p\pi^+\pi^-$ invariant mass distributions are identical within statistical limits and are shown combined in Figure 20a at 2.4 GeV/c and 20c at 2.9 GeV/c. No outstanding enhancements are seen in the 2.9 GeV/c data or in that at 2.7 GeV/c (20, 27), although there are possible small effects at 2.7 GeV/c in the regions 1400 to 1450 MeV and 1600 to 1700 MeV. In the 2.4 GeV/c data there appears to be an effect in the region 1440 to 1520 MeV.

The presence of a resonance decaying to $\bar{p}\pi^+\pi^-$ or $p\pi^+\pi^-$ would be inconsistent with the conclusion that Reaction 1 is dominated by nearly 100% $\overline{\Delta^{++}}\,\Delta^{++}$ production. However, in a recent study of the reaction $\bar{p}p(n) \rightarrow \bar{p}p\pi^+\pi^-(n)$ at 2.8 GeV/c by Bacon et al. (3), effects were reported in the $\bar{p}\pi^+\pi^-$ and $p\pi^+\pi^-$ mass distributions. These effects were assigned masses of 1400 ± 10 MeV and widths of 80 ± 20 MeV. It was also reported that resonance production ($\overline{\Delta^{++}}\,\Delta^{++}$ plus some single resonance production) accounts for only 72% of the events at 2.8 GeV/c. Since these findings are not in agreement with the 2.7 and 2.9 GeV/c results, an investigation was done (20) to determine whether the $\bar{p}\pi^+\pi^-$ and $p\pi^+\pi^-$ invariant mass distributions at 2.7 and 2.9 GeV/c could be explained by the double-isobar one-pion-exchange model. The conclusion was that the model does give an adequate representation of the data and that Reaction 1 proceeds essentially 100% through the $\overline{\Delta^{++}}\,\Delta^{++}$ channel at both momenta. Ferbel et al. (6) found that a similar calculation gives an acceptable representation of the data for Reaction 1 at 3.28 and 3.66 GeV/c. The calculations given in Reference 20 are summarized here, and a comparison with the 2.4 GeV/c data is in-

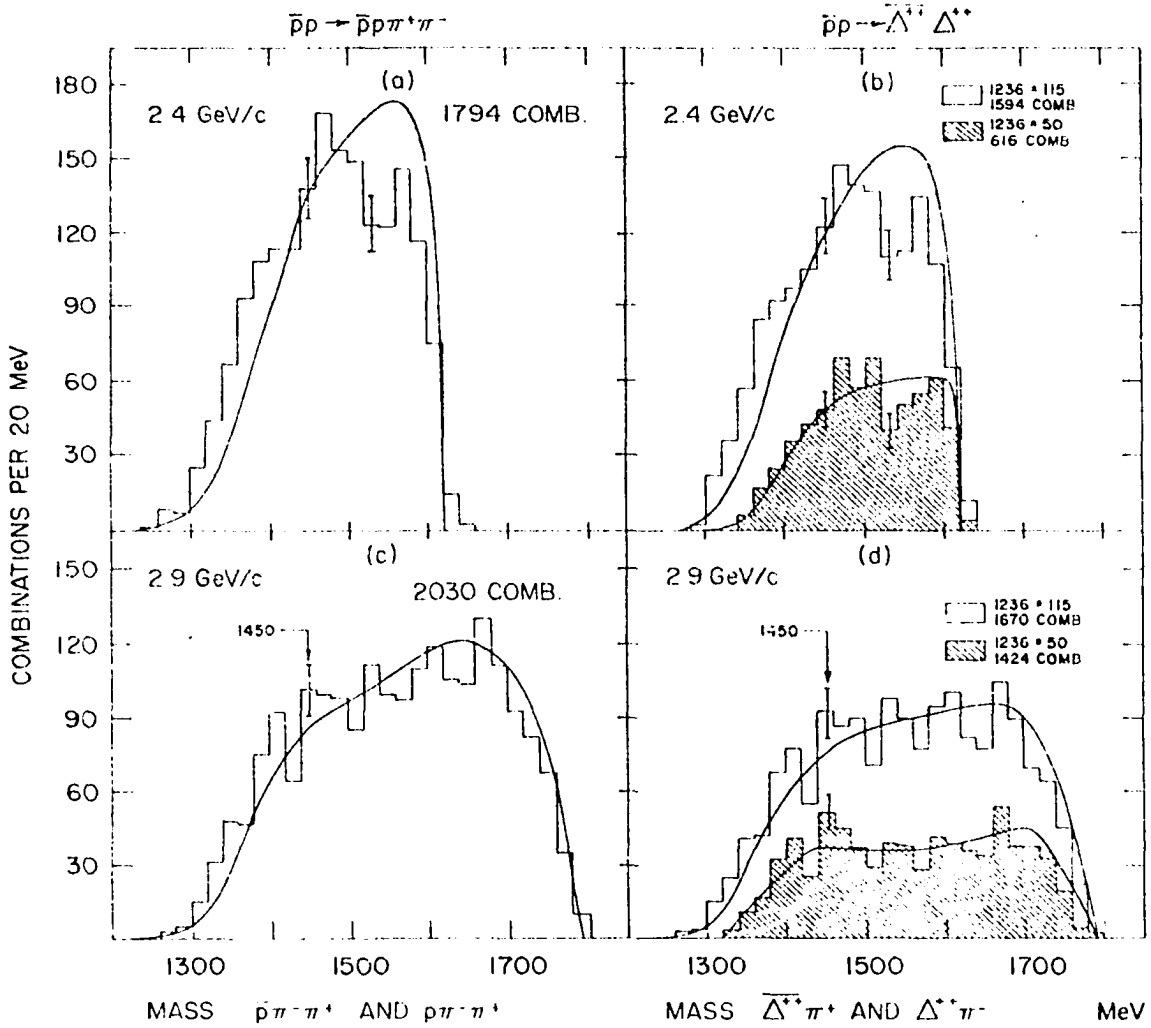

Figure 20. a), c) The combined $\bar{p}\pi^-\pi^+$ and $p\pi^-\pi^+$ invariant mass distributions. b), d) The same distributions for events having the $\bar{p}\pi^-$ and $p\pi^+$ invariant masses in the Δ region (defined as 1236 ± 115 MeV for the open histograms and 1236 ± 50 MeV for the shaded histograms). The solid curves are the predictions of the double-isobar OPE model normalized to the data.

cluded.

The differential cross-section with respect to u according to the model is

$$\frac{d\sigma}{du} = \frac{1}{4\pi^3 F^2} \int \Omega(\bar{\omega}, \omega, \Delta^2) P(u; m^2, \omega^2)$$

$$\times \bar{\omega}^2 \frac{d\sigma_1}{d\Omega} (\bar{\omega}, \cos\bar{\theta}) \frac{1}{(\Delta^2 + m^2)^2}$$

$$\times \omega^2 \sigma_1 (\omega) P(\omega; M^2, m^2)$$

$$\times d\omega \, dt^2 \, d\cos\theta_2^P \, d\phi_2^P \, . \qquad (20)$$

In this expression $d\sigma_1/d\Omega$ is the differential cross-section for $\bar{p}\pi^- \to \bar{p}\pi^-$ scattering at center-of-mass energy $\bar{\omega}$ and center-of-mass scattering angle $\bar{\theta}$, given by

$$\frac{d\sigma_1}{d\Omega} (\bar{\omega}, \cos\bar{\theta}) = \sigma_1 (\bar{\omega}) \frac{1 + 3\cos^2\bar{\theta}}{8\pi} \, , \qquad (21)$$

where $\sigma_1(\bar{\omega})$ is given by Equation 19 with ω replaced by $\bar{\omega}$ throughout. The variables and limits of integration are defined in Reference 15. Briefly, t^2 is the square of the four-momentum transferred from the incident $\bar{p}$ to the outgoing $\bar{p}$, while θ_2^P and ϕ_2^P are the polar and azimuthal scattering angles of the final $p\pi^+$ system in the $p\pi^+\pi^-$ rest frame, with the direction of the incident p taken as the z axis. The remaining quantities are the same as in Expression 18.

The predictions of the double-isobar model for the $\bar{p}\pi^+\pi^-$ and $p\pi^+\pi^-$ invariant mass distributions, given by Equation 20, are shown normalized to the data in Figures 20a and 20c for the two momenta. In order to consider the possibility of a small non-resonant background, cuts were made

in the data to include only those events in a restricted $\overline{\Delta^{++}}$ Δ^{++} mass region. Corresponding cuts were made in the calculation. The data having both $\bar{p}\pi^-$ and $p\pi^+$ invariant masses in 1236 ± 115 MeV and in the more restricted region 1236 ± 50 MeV are shown in Figures 20b and 20d at 2.4 and 2.9 GeV/c, respectively. The corresponding calculated distribution is shown normalized to the data in each case.

The agreement is seen to be quite good at 2.9 GeV/c, and is also good at 2.7 GeV/c (20). However the model does not represent the data well at 2.4 GeV/c.

The $\bar{p}\pi^+\pi^-$ and $p\pi^+\pi^-$ mass distributions were also examined for events having <u>either</u> the $\bar{p}\pi^-$ or $p\pi^+$ mass outside the Δ region, and for events having <u>both</u> $\bar{p}\pi^-$ and $p\pi^+$ masses outside the Δ region. While the numbers of events meeting these requirements are limited, both of these restrictions yielded $\bar{p}\pi^+\pi^-$ and $p\pi^+\pi^-$ mass distributions at 2.4 GeV/c which lacked the apparent enhancement in the 1440 to 1520 MeV region. Apparently this effect is associated with the double-resonance production. Further evidence of this comes from the prediction of phase-space, which is peaked well above 1520 MeV.

It was noted that the calculations are rather sensitive to the energy-dependent width used in Expression 19. A good representation of the real π^+p elastic scattering data was necessary to get good predictions of the $\bar{p}\pi^+\pi^-$ and $p\pi^+\pi^-$ mass distributions at 2.7 and 2.9 GeV/c. The failure of the model to predict the $\rho_{1,1}$ density matrix element was found to be of little consequence, however. The predictions using $1 + 3\cos^2\theta$ ($\rho_{1,1} = 0.5$) in Expression 21 were changed only very slightly by using 1 ($\rho_{1,1} = 0.25$).

VI. CONCLUSION

The cross-section for Reaction 1 is 1.48 ± 0.07 mb at 2.4 GeV/c and 2.53 ± 0.10 mb at 2.9 GeV/c. A compilation of the reported cross-sections for this reaction is shown in Figure 21. The cross-section is seen to rise rapidly from the $\overline{\Delta^{++}}\,\Delta^{++}$ threshold to a maximum of 3.8 mb at 3.6 GeV/c, then fall slowly. The data are consistent with nearly 100% double resonance production at 2.4, 2.7, and 2.9 GeV/c. The fraction of $\overline{\Delta^{++}}\,\Delta^{++}$ production is difficult to discuss as a function of beam momentum because of the several different methods used to determine it in the various experiments. Only the 63% figure of Alles-Borelli *et al.* (12) at 5.7 GeV/c was obtained by the method used here. (Some other experimenters have simply counted events in a restricted $\overline{\Delta^{++}}\,\Delta^{++}$ mass region.) Nevertheless, the reported values are presented in Figure 21 for comparison with the predictions of the double-isobar one-pion-exchange model. These predictions are too large near threshold, while the data are not consistent enough to give a significant test at higher momenta. If only the values of the $\overline{\Delta^{++}}\,\Delta^{++}$ cross-section which were determined by the present method are considered, the model prediction is seen to be a good representation of the data at 5.7 GeV/c, becoming increasingly too large as threshold is approached. It is of interest to note that replacing the form-factors used here by those of Ferrari and Sellari (15) results in a calculated cross-section which is just slightly smaller than the experimental value at 2.7 GeV/c (2). However the discrepancy with the data becomes larger at higher beam momenta, and other aspects of the data are not as well reproduced as they are with the present form-factors.

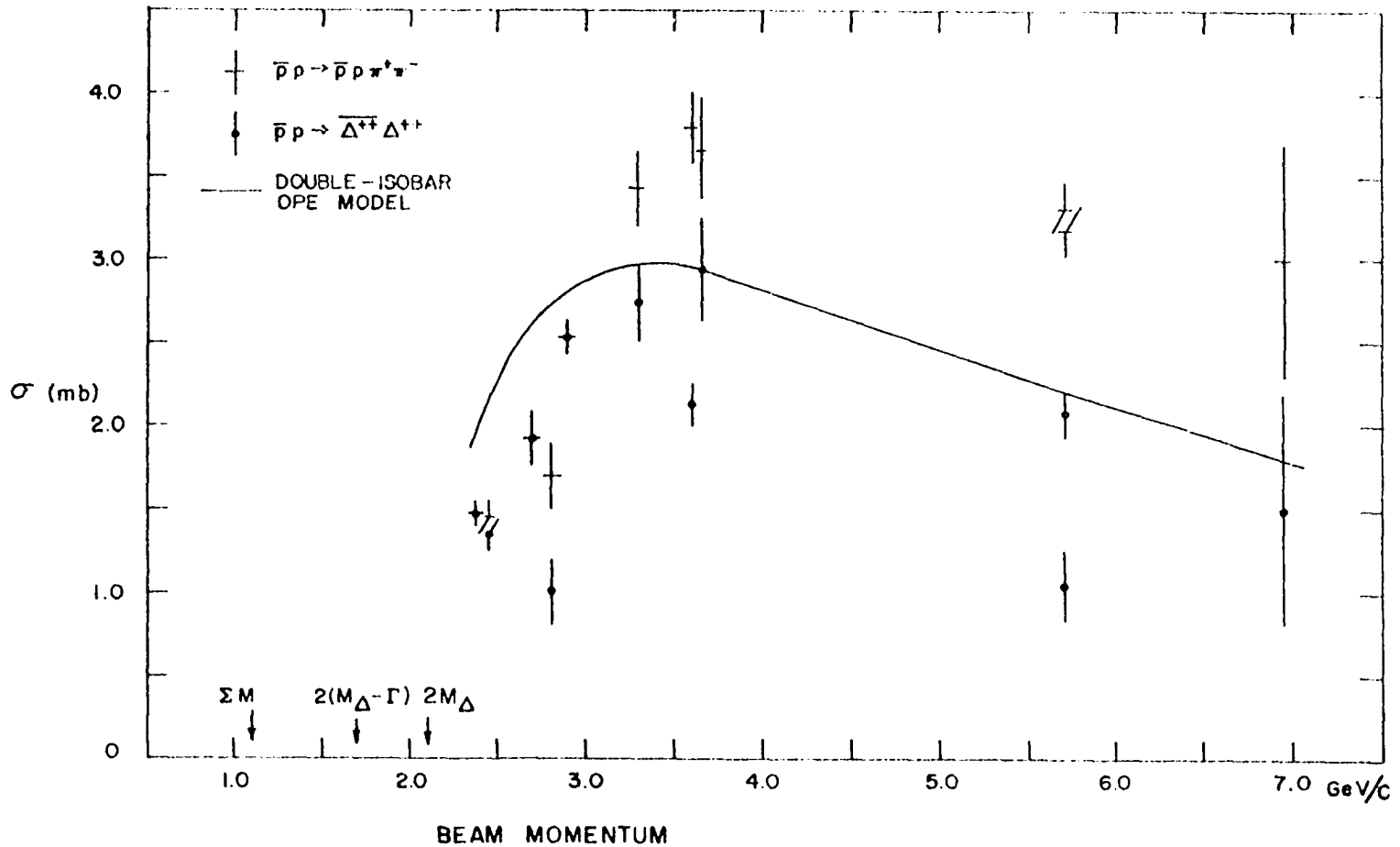

Figure 21. The cross-sections for Reactions 1 and 2 as functions of beam momentum. The data are from References 1 through 13 and the present report. Also shown is the prediction of the double-isobar OPE model for Reaction 2.

Reaction 1 is peripheral at both 2.4 and 2.9 GeV/c, the distribution of the center-of-mass scattering angle being peaked near $\cos\theta_p = 1$. This peak becomes sharper with increasing beam momentum. Wolf (28) has shown that this effect is consistent with the double-isobar one-pion-exchange model. In contrast, the decay angular distributions are not well predicted by the model.

The $\rho_{1,1}$ spin-density matrix element has a strong dependence on the square of the four-momentum transfer, falling at each momentum reported here from near the predicted value of 0.5 at $\Delta^2 = 0$ to about 0.2 in the region $\Delta^2 \sim 0.6$ $(GeV/c)^2$, then rising again for larger Δ^2. A similar behavior is seen in the data at higher momenta, where it has been explained in terms of the one-pion-exchange model with absorption (32). No correlation in the $\overline{\Delta^{++}}$ and Δ^{++} production is indicated by the joint spin-density matrix elements reported here. Small correlations were observed at 5.7 GeV/c (12).

The double-isobar one-pion-exchange model gives a good representation of the Δ^2 distribution, but a somewhat less satisfying prediction of the $\bar{p}\pi^-$ and $p\pi^+$ invariant mass distributions. The predictions for both distributions are better at 2.9 GeV/c than at 2.4 GeV/c. The predictions of the $\bar{p}\pi^+\pi^-$ and $p\pi^+\pi^-$ invariant mass distributions are acceptable at 2.9 GeV/c, but are not at all good at 2.4 GeV/c. It is clear that the form-factor one-pion-exchange model, though accurate in some of its predictions, is not completely adequate for describing the data. Even the addition of absorption corrections is not sufficient to bring the model predictions into agreement with the near-threshold data (2). It is hoped that the

data presented here will provide an incentive for additional theoretical calculations.

VII. BIBLIOGRAPHY

1. P. Mason, H. Muirhead, A. Poppleton, K. Whiteley, R. Rigopoulos, P. Tsilimigras, and A. Vayaki-Serafimidu, The process $pp \rightarrow \Delta\Delta$ at 2.5 GeV/c. Unpublished preliminary report presented at the Lund International Conference on Elementary Particles, Lund, Sweden, June, 1969. Department of Physics, University of Liverpool, Liverpool, England.

2. H. B. Crawley, R. A. Leacock, and W. J. Kernan, Phys. Rev. 154, 1264 (1967).

3. T. C. Bacon, F. Bomse, T. B. Borak, T. B. Cochran, W. J. Fickinger, E. R. Goza, H. W. K. Hopkins, and E. O. Salant, Phys. Rev. Letters 22, 43 (1969).

4. T. Ferbel, J. Sandweiss, H. D. Taft, M. Gailloud, T. E. Kalogeropoulos, T. W. Morris, and R. M. Lea, Phys. Rev. Letters 9, 351 (1962).

5. T. Ferbel, A. Firestone, J. Sandweiss, H. D. Taft, M. Gailloud, T. W. Morris, W. J. Willis, A. H. Backmann, P. Baumel, and R. M. Lea, Phys. Rev. 138, B1528 (1965).

6. T. Ferbel, R. Holmes, and S. Stone, Phys. Rev. Letters 22, 1141 (1969).

7. H. C. Dehne, E. Raubold, P. Söding, M. W. Teucher, G. Wolf, and E. Lohrmann, Phys. Letters 9, 185 (1964).

8. H. C. Dehne, E. Lohrmann, E. Raubold, P. Söding, M. W. Teucher, and G. Wolf, Phys. Rev. 136, B843 (1964).

9. K. Böckmann, B. Nellen, E. Paul, I. Borecka, J. Diaz, U. Heeren, U. Liebermeister, E. Lohrmann, E. Raubold, P. Söding, S. Wolff, S. Coletti, J. Kidd, L. Mandelli, V. Pelosi, S. Ratti, and L. Tallone, Phys. Letters 15, 356 (1965).

10. K. Böckmann, B. Nellen, E. Paul, B. Wagini, I. Borecka, J. Diaz, U. Heeren, U. Liebermeister, E. Lohrmann, E. Raubold, P. Söding, S. Wolff, J. Kidd, L. Mandelli, L. Mosca, V. Pelosi, S. Ratti, and L. Tallone, Nuovo Cimento 42, 954 (1966).

11. V. Alles-Borelli, B. French, Å. Frisk, and L. Michejda, Nuovo Cimento 47, 232 (1967).

12. V. Alles-Borelli, B. French, Å. Frisk, and L. Michejda, Nuovo Cimento 48, 360 (1967).

13. T. Ferbel, A. Firestone, J. Johnson, J. Sandweiss, and H. D. Taft, Nuovo Cimento 38, 19 (1965).

14. W. A. Cooper, in Symposium on Nucleon-Antinucleon Interactions, Argonne National Laboratory, Argonne, Illinois, May, 1968. Argonne National Laboratory Report ANL/HEP 6812, p. 123.

15. E. Ferrari and F. Sellari, Nuovo Cimento Suppl. 24, 453 (1962).

16. J. D. Jackson, Rev. Mod. Phys. 37, 484 (1965).

17. H. P. Dürr and H. Pilkuhn, Nuovo Cimento 40A, 899 (1965).

18. R. A. Jespersen, W. J. Kernan, and R. A. Leacock, (Abstract) Bull. Am. Phys. Soc. 14, 181 (1969).

19. R. A. Jespersen, W. J. Kernan, and R. A. Leacock, Pion production without annihilation in pp interactions at 2.9 GeV/c. Unpublished preliminary report presented at the Lund International Conference on Elementary Particles, Lund, Sweden, June, 1969. Department of Physics, Iowa State University of Science and Technology, Ames, Iowa.

20. W. J. Kernan, H. B. Crawley, R. A. Jespersen, and R. A. Leacock, Phys. Rev. (to be published).

21. R. P. Radlinski and W. J. Kernan, Antiproton-proton annihilations at 2.4 and 2.9 GeV/c. Unpublished preliminary report presented at the Lund International Conference on Elementary Particles, Lund, Sweden, June, 1969. Department of Physics, Iowa State University of Science and Technology, Ames, Iowa.

22. W. J. Higby and A. H. Klein, U.S.A.E.C. Ames Laboratory on-line control system for bubble chamber film measuring. Report to be published. Department of Physics, Iowa State University of Science and Technology, Ames, Iowa. (ca. 1969).

23. J. P. Berge, F. T. Solmitz, and H. D. Taft, Rev. Sci. Instr. 32, 538 (1961).

24. W. J. Kernan, W. J. Higby, and I. H. Boessenroth, United States Atomic Energy Commission Report IS-1072 [Iowa State University Science and Technology, Ames, Iowa. Institute for Atomic Research] (1964).

25. A. Pais, Phys. Rev. Letters 3, 242 (1959).

26. J. D. Jackson, Nuovo Cimento 34, 1644 (1964).

27. H. B. Crawley, Unpublished Ph.D. thesis. Library, Iowa State University of Science and Technology, Ames, Iowa, (1966).

28. G. Wolf, Phys. Rev. Letters 19, 925 (1967).

29. K. Gottfried and J. D. Jackson, Nuovo Cimento 33, 309 (1964).

30. H. Pilkuhn and B. E. Y. Svensson, Nuovo Cimento 38, 518 (1965).

31. E. Ferrari, Nuovo Cimento 30, 240 (1963).

32. B. E. Y. Svensson, Nuovo Cimento 39, 667 (1965).

33. M. Gell-Mann and K. M. Watson, Ann. Rev. Nucl. Sci. 4, 219 (1954).

34. M. N. Focacci and G. Giacomelli, Pion-Proton Elastic Scattering. European Council for Nuclear Research Report CERN 66-18 [CERN, Geneva, Switzerland] (1966).

VIII. ACKNOWLEDGEMENTS

The author wishes to express his gratitude to Professor W. J. Kernan for his personal interest and assistance in all aspects of this investigation. He also wishes to express sincere thanks to Professor R. A. Leacock for his guidance in the theoretical interpretation of the data. The many discussions with both of them were invaluable.

Appreciation is expressed to the scanning and measuring staff directed by Mrs. Betty Pepper for their many hours of work, without which this investigation would not have been possible.

The assistance of the programming staff headed by Mr. W. J. Higby and many helpful discussions of programming problems with Mr. T. L. Schalk greatly reduced the time required to complete this study. Their help is greatly appreciated.

The author also wishes to express his gratitude for the financial support given him: a National Defense Education Act Fellowship for 1965-68, and a National Aeronautics and Space Administration Fellowship for 1968-69.

Acknowledgement is given to Professors L. S. Schroeder and W. L. Talbert for reading the manuscript and offering helpful suggestions.

Finally, special thanks go to the author's wife, Sandy, for her encouragement and support throughout his student years.